Title: Pulsatory response of the BcLOV4 photoreceptor through intramolecular feed-forward regulation

Authors: Zikang (Dennis) Huang[1], Malvin Forson[2,3], William Benman[1], Kevin H. Gardner[2,3,4,5,6,*], Lukasz J. Bugaj[1,7,8,*]

***co-corresponding author**

Affiliations:
[1]Department of Bioengineering, University of Pennsylvania, Philadelphia, PA, 19104, USA
[2]Structural Biology Initiative, CUNY Advanced Science Research Center, New York, NY 10031
[3]PhD Program in Biochemistry, The Graduate Center, City University of New York, New York, NY 10016
[4]Department of Chemistry and Biochemistry, City College of New York, New York, NY, 10031, USA
[5]PhD Program in Chemistry, The Graduate Center, City University of New York, New York, NY 10016
[6]PhD Program in Biology, The Graduate Center, City University of New York, New York, NY 10016
[7]Institute for Regenerative Medicine, University of Pennsylvania, Philadelphia, PA, 19104, USA
[8]Abramson Cancer Center, University of Pennsylvania, Philadelphia, PA, 19104, USA

***Contact Information**
bugaj@seas.upenn.edu, kgardner@gc.cuny.edu

One-Sentence Summary: Individual proteins can dynamically encode information through interactions between their component domains, revealing principles for complex signal processing in natural and engineered proteins.

Abstract
Biomolecular networks can dynamically encode information, generating time-varying patterns of activity in response to an input. Here we find that dynamic encoding can also be performed by individual proteins. BcLOV4 is an optogenetic protein that uniquely displays pulsatory activation in response to a step input of light, and response dynamics can be shaped by both light and temperature. However, how the BcLOV4 protein generates this step-to-pulse response is not understood. Here we combined live cell imaging and simulations to find that the activity pulse results from an intramolecular incoherent feedforward loop (IFFL) implemented by competitive interactions between protein domains that separately respond to light or temperature. We identified these light- and temperature-sensitive regions and found that they implement the IFFL by competitively caging an activation region. Structural and sequence analysis revealed temperature-responsive regions of BcLOV4 which allowed experimental tuning of activation dynamics and suggested that tuning has also occurred throughout evolution. These findings enabled the generation of more thermostable optogenetic tools and identified a modular thermosensitive domain that endowed thermogenetic control over unrelated proteins. Our findings uncover principles of dynamic and combinatorial signal processing in individual proteins that will fuel development of more sophisticated and compact synthetic systems.

Introduction

Proteins serve as information processors in the cell, integrating combinations of internal and environmental cues to execute an appropriate response (*1*). Engineered proteins can perform complex information processing, for instance through logic gates that drive an output based on combinations of steady-state intramolecular interactions or allostery (*2–4*). In principle, proteins could also process information with non-steady-state computation like dynamic encoding, where input information is transduced into a temporal pattern of an output. However, to date dynamic encoding has generally not been recognized within individual proteins.

Dynamic encoding is commonplace, however, within networks of proteins (*5*). One prominent class of networks generates transient pulses, a ubiquitous type of biomolecular signal that plays many roles including to limit duration of response, increase dynamic range, or enable temporal encoding of information(*6*). The broad utility of step-to-pulse responses likely underlies their appearance across essential cell behaviors like response to growth factors(*7*), adaptation to stress(*8–10*), and recognition of chemical gradients (*11*). Corrupted pulsatory responses of signaling, in turn, have been associated with disease including cancer (*12*).

Networks can achieve pulsatory responses using feedback or feedforward regulation. One such pattern is the incoherent feed-forward loop (IFFL) (*13*), a 3-node motif where an input node stimulates an output node but also stimulates an inhibitory node that subsequently suppresses the output. This arrangement results in a pulse of output activity in response to persistent input. The IFFL can achieve processing behaviors that include perfect adaptation(*6*, *14*), fold-change detection(*15*), and signal acceleration (*16*). IFFL behavior could conceivably also be achieved by individual proteins, for example through intra-molecular domain interaction networks, though such behavior has not been previously described.

Here we explore the potential for such regulation within the BcLOV4 photoreceptor, an optogenetic protein that shows pulsatory activity in response to constant blue light in heterologous cells(*17*, *18*). Upon stimulation, BcLOV4 both clusters and translocates to the plasma membrane within seconds but subsequently dissociates within tens of minutes despite persistent illumination(*18*, *19*). Uniquely, its pulsatile kinetics can be tuned by temperature: dissociation is slow at low (room) temperatures but becomes increasingly rapid between 30-40°C. Thus BcLOV4 converts two independent sensory inputs into a tunable pulse of multiple outputs. However, the mechanistic basis for BcLOV4 pulses is not understood.

Using a combination of *in vitro,* cellular, and *in silico* approaches, we show that BcLOV4 achieves pulse generation as a single protein using an intramolecular IFFL based on competitive interactions between sensory domains that respond to either light or temperature. Light rapidly triggers the active membrane-associated state but also licenses an autoinhibitory temperature-inactivating (TI) domain that more slowly suppresses this activity. A thermodynamic model of the IFFL described this behavior and predicted non-intuitive consequences of mutations and conditions that perturbed the energetics of the underlying protein states. We then uncovered the identity of the relevant domains and their interactions, finding a multimerization region that is essential for membrane binding, as well as a modular TI domain that competes with the light-sensitive (LS) domain for regulation of this multimerization/activation region. Our work reveals principles of how individual proteins can implement dynamic signal processing, discovers a compact temperature-sensing protein module, and uncovers molecular determinants of thermo-sensing that can be harnessed to engineer novel light- or temperature-sensitive probes.

Results

BcLOV4 activation dynamics can be explained by incoherent feed-forward regulation within its globular domains.

BcLOV4 is a 595 amino acid protein comprising three main globular domains: 1) an N-terminal regulator of G-protein signaling (RGS) domain, 2) a light-sensing light-oxygen-voltage (LOV) domain, and 3) a C-terminal domain of unknown function (DUF) (**Figure 1A**). Together, these domains implement a multi-input/multi-output protein: BcLOV4 responds to both light and temperature, and it both oligomerizes and translocates to the plasma membrane in response (*18*, *19*). Unique among known photoreceptors, BcLOV4 transduces a constant light input into a pulse of activity whose kinetics are a function of temperature. In mammalian cells, light stimulation triggers translocation of BcLOV4 to the plasma membrane through electrostatic interactions of an amphipathic helix (AH1) located between the LOV and DUF domains (**Figure 1A**)(*17*, *20*). Within ~10 minutes, however, BcLOV4 begins to dissociate from the membrane and returns to the cytoplasm at a rate that increases with temperature, despite the continued presence of the light stimulus (**Figure 1B,C, Movie S1**)(*18*). If subsequently maintained under high temperature (30-40°C), BcLOV4 will remain cytoplasmic and not respond to light (*18*). However, the protein can be reset to its light-responsive state by lowering the temperature (*10*).

Key mechanistic questions remain regarding the above sequence of events. First, how are the multiple inputs coordinated on a molecular level to yield the observed pulsatile dynamics? Second, how does the active state result in membrane binding, and what is the role of BcLOV4 oligomerization? And third: what is the molecular basis for temperature sensing and thermal inactivation? (**Figure 1B**)

To understand the pulsatory response to light, we hypothesized that the modular domains within BcLOV4 implement an incoherent feed-forward loop (IFFL), analogous to pulse-generation networks found in the context of gene expression and sensory adaptation (*21*). In this proposed model, illumination triggers the light-sensitive (LS) domain to expose an activation domain but also licenses inhibition of this activation domain by a hypothetical temperature-inactivating (TI) domain on a slower time scale (**Figure 1D**). We described the above interactions as three major states (light-sensitive, active, and temperature-inactivated) and the transitions between them using a thermodynamic model (**Figure 1E**). At baseline (dark, high temp.), the LS and TI states have lower energy levels than the active state and determine the starting equilibrium. Addition of blue light destabilizes the LS state, representing the well characterized photocycle of LOV domains (*22*). In parallel, increasing the temperature stabilizes the TI state (**Figure 1E, F**). We modeled this system with ordinary differential equations (see methods), adding rates of protein synthesis and degradation as well as a slow rate of entry to an irreversibly inactivated state to account for prior observations of incomplete reversibility after long-term exposure to light under high (37-40°C) temperature (*10*)(**Figure S1**).

The thermodynamic model predicted BcLOV4 activation dynamics: under high temperatures, light induced rapid activation and subsequent slower inactivation that ultimately populated the low-energy TI state, recapitulating pulsatile activation (**Fig 1F**). Decreasing temperature disfavored the TI state, resulting in more persistent activation, and the degree of persistence decreased monotonically with increasing temperature (**Figure 1G**). These increasingly transient pulses were confirmed by observing BcLOV4 translocation after light stimulation at temperatures ranging from 31-39°C (**Figure 1H**). The model also predicted that, starting from the TI

state, a step decrease in temperature would populate the membrane-bound (active) state as an increasing function of light intensity (**Fig 1I**). This prediction was supported by experiments where BcLOV4 was first pushed to the TI state by pre-illumination at high temperatures, followed by a drop in temperature at various levels of light, with higher light yielding higher cold-induced membrane binding (**Figure 1J**).

Experimental validation of the thermodynamic IFFR model

Our model further made three surprising predictions. First, in contrast to a prior study that suggested that entry into the temperature-inactivated (TI) state could only happen after light stimulation (*18*), our present model predicted that the LS, active, and TI states exist in equilibrium (**Figure 2A,B**). We thus asked whether we could shift the distribution of protein from the LS to the TI state by increasing temperature in the *dark*, which would manifest in lower membrane localization directly after light stimulation. Indeed, the amount of maximal translocation under light stimulation (at 3.5 min) decreased monotonically with increased temperature, consistent with BcLOV4 equilibration between states in the absence of light (**Figure 2C-D, S2A-B**).

A second prediction was that stabilization of the active state should decrease the rate of thermal inactivation (**Figure 2E-F**). We stabilized the active state through mutation of the critical LOV cysteine (C292 in BcLOV4) which forms a covalent adduct with the C4a carbon of a photoexcited flavin mononucleotide (FMN) cofactor (*23*). Natural or engineered LOV domains that lack this critical cysteine can still be photoactivated through alternative photochemistry, likely the formation of a FMN neutral semiquinone (NSQ) that has substantially longer dark-reversion kinetics relative to the canonical quinone form, indicating a more stable form of the active state (*24*). Consistent with this prediction, BcLOV4 variants containing either a C292A or C292P mutation remained membrane localized at high temperatures (37°C), substantially longer than wildtype wt BcLOV4, with strong localization still observed after more than 10 hrs of stimulation (**Figure 2G-H**) (*25*). Importantly, these C292A/P mutations also resulted in measurable basal (dark) levels of membrane localization, consistent with model predictions (**Figure S3**) (*24*). The kinetics of light activation were also slowed for the C292A/P mutants, consistent with an increased energy barrier for transition to the active state, as previously observed (**Figure 2G-H**) (*24*, *26*).

One final and non-intuitive prediction from our three-state model was on the effect of mutations that destabilize the LS state. Studies of a canonical LOV domain, AsLOV2, revealed that photochemical triggering of LOV domains leads to the release of auxiliary alpha-helices (A'α, Jα) from positions on the LOV domain core as part of the activation process (*22*, *27*). An analogous Jα helix is seen in secondary structure predictions of BcLOV4 (*17*), suggesting that mutations that weaken the docking of the Jα helix onto the LOV domain core would destabilize the LS state. In a normal 2-state LOV photo-switch, such mutations would result in higher basal levels of activated protein that could be further maximally stimulated with light. However, the BcLOV4 model predicts higher basal levels but a *decreased* maximal stimulation amplitude because the equilibrium of the mutants would push more protein to the TI state even in the dark (**Figure 2I-J**). We tested this prediction with two individual mutations, L335A or Y337A, that alter residues predicted to contribute to interactions between the core LOV domain and Jα helix (*24*). Indeed, both mutants showed slightly elevated basal (dark) membrane localization and *lower* maximal amplitude of light-induced membrane translocation compared to wt BcLOV4, in agreement with model predictions (**Figure 2K, S4**).

Collectively, these series of experiments validate the IFFR model of BcLOV4 regulation and confirm that a dynamic equilibrium between three states can successfully capture both known and novel, non-intuitive activation dynamics.

Regulated avidity of AH1 is necessary and sufficient for BcLOV4 membrane translocation

We next set out to identify the protein domains and molecular mechanisms that govern each of the model states. Photo-sensing is clearly mediated by the LOV domain, consistent with prior mechanistic studies as well as with our mutational studies in this report (**Figure 2**) (*17*). However the mechanism of the BcLOV4 active state was less well defined from these works, including understanding whether the two functional outputs— membrane translocation and clustering— are somehow coordinated (**Figure 1B, 3A,B**) (*17*, *19*). It was initially proposed that light-induced unfolding of the Jα helix revealed an amphipathic helix (AH1) that provided affinity for the membrane (**Figure S5A**) (*17*). However, several observations counter this model. First, a short fluorescently tagged AH1 fragment does not visibly localize to the membrane, suggesting that exposure of AH1 itself is insufficient for translocation (**Figure S5B**). Alternatively, AH1 could contribute to membrane binding by providing weak affinity that is strengthened when combined with additional weak interactions (high avidity). In support of this mechanism, a fusion of AH1 to another weak membrane-binding motif—a polybasic fragment from the STIM1 (referred as STIM1 in the rest of the paper) protein (*28*)—localized to the membrane, even though both AH1 and the STIM1 fragment alone were cytosolic (**Fig S5**). Furthermore, a fusion of this STIM1 fragment to full-length BcLOV4 localized to the membrane even in the dark, suggesting that dark-state BcLOV4 in the absence of STIM already has a weak propensity for membrane binding. Importantly, the dark-state membrane association of BcLOV4-STIM1 was lost if positively-charged amino acids in AH1 were removed (**Fig S5)**. This result argues that AH1 may in fact be exposed in the dark (**Figure S5C-D**). Interestingly, the BcLOV4-STIM1 fusion gradually falls off the membrane during light stimulation at 37°C (**Figure S6**), suggesting that although AH1 may not be occluded in the dark, it may be occluded as part of the thermal response that is only licensed after light stimulation. Accordingly, the L335A or Y337A mutations that weaken LOV-Jα undocking and partially mimic light stimulation *reduced* membrane localization of BcLOV4-STIM in the dark, further supporting our 3-state thermodynamic model (**Figure S7**). Collectively, these results suggest that the critical AH1 domain may in fact remain exposed in the LS (dark) state but is caged upon entry to the TI state.

How could light stimulation drive membrane translocation if AH1 is already exposed in the dark? We asked whether light-induced clustering provided a mechanism for enhancing AH1 avidity and resultant translocation. BcLOV4 can cluster in the absence of membrane binding upon mutation of the AH1 region (BcLOVclust(*20*)), suggesting that clustering might precede membrane translocation(*19*, *20*). In support, live-cell imaging with sufficiently high magnification and 1 Hz frame rate showed rapid cluster formation in the cytoplasm within seconds of light stimulation, followed by a subsequent loss of clusters and simultaneous increase in accumulation at the membrane (**Figure S9, Movie S2**). To test whether clustering was necessary for translocation, we fused *E. coli* maltose binding protein (MBP), a solubilization tag known to suppress protein condensation and assembly, to the N-terminus of BcLOV4 (**Figure 3C**) (*29*). MBP-BcLOV4 showed markedly weaker photoactivated translocation compared to wt BcLOV4 at 25°C and completely abrogated translocation at 37°C, further suggesting a causal role for oligomerization (**Figure 3C-E, S8**). We then tested the sufficiency of clustering by grafting the AH1 region to an orthogonal

clustering module, Cry2 (**Figure 3F-G**) (*30*). Light-activated AH1-Cry2 rapidly translocated to the plasma membrane, whereas a mutant lacking two AH1 lysines involved in membrane interactions formed only cytoplasmic clusters (**Figure 3H-I, Movie S3**). Next, we asked whether clustering of BcLOV4 itself was sufficient to drive membrane binding through avidity of a weak membrane-binding domain (**Figure 3J**). We thus fused the STIM1 polybasic domain to the C-terminus of BcLOVclust. Light stimulation indeed drove the fusion protein to the membrane, whereas BcLOVclust alone formed clusters in the cytoplasm (**Figure 3K-L, S10**) (*20*). Together, our studies argue that light induces conformational changes in BcLOV4 that promotes its clustering, which is both necessary and sufficient for the observed membrane translocation that occurs through increased avidity of weak membrane-binding domains.

Electrostatic interactions in Jα-AH1 mediate clustering.

Our conceptual model implies the existence of a photo-regulatable region that controls clustering. Because LOV domain effectors commonly reside in or downstream of the C-terminal Jα helix, we examined the sequence around this C-terminal region and found patches of charged amino acids (**Figure 3M-N**), a pattern found to promote self-assembly in other protein contexts (*31*, *32*). We thus asked whether this region, spanning from the Jα helix to the first 20 amino acids on the N-terminus of the Domain of Unknown Function (Jα-AH1-DUF(N)) was sufficient to promote clustering. While a fusion of this region to GFP appeared diffuse, co-expression with a cluster-amplifying CluMPS reporter(*33*) yielded puncta, indicating that Jα-AH1-DUF(N) formed submicroscopic assemblies (**Figure 3O**). As further validation, we fused Jα-AH1-DUF(N) to a fluorescently tagged FTH1, a 24-meric subunit of ferritin (**Figure 3P**) (*34*). While FTH1-mCherry alone appeared diffuse, addition of Jα-AH1-DUF(N) resulted in micron-scale puncta, further supporting self-interaction potential of the added region (**Figure 3Q-R**). Substitution of positively-charged arginine residues in Jα with alanines eliminated this clustering potential (**Figure 3Q-R).** Furthermore, mutating 3 lysines in AH1 to negatively charged glutamic acids enhanced clustering, but only in the presence of the Jα, further confirming the dependence of clustering on the charge balance in this region **(Figure S11**) (*35*). Collectively, these results depict a model where light-induced exposure of the Jα helix reveals critical charged residues that promote clustering and subsequent membrane translocation of BcLOV4.

The DUF domain mediates temperature sensing

Finally, we sought to understand the molecular nature of the temperature-inactivated (TI) state. Since Jα is caged in the LS state and the adjacent AH1 is caged in the TI state but itself is not sensitive to temperature (**Figure S5B**), we reasoned that IFFL regulation could result from competitive caging of the Jα-AH1 active region via two distinct interactions, one regulated by light (by the LOV domain, upstream of Jα-AH1) and the other by temperature. We thus looked for the temperature sensor directly downstream of Jα-AH1, in the C-terminal Domain of Unknown Function (DUF) (**Figure 4A-C**). To determine whether DUF contributes to thermo-sensing, we compared membrane localization of the AH1-FTH1 construct in the presence or absence of DUF downstream of AH1. Remarkably, whereas AH1-FTH1 bound the membrane at both high and low temperatures, AH1-DUF-FTH1 bound the membrane at 25°C but not at 37°C (**Figure 4D-F**). Furthermore, addition of the Jα helix upstream of AH1 (Jα-AH1-DUF-FTH1) prevented membrane binding at any temperature, despite the continued avidity provided by FTH1 multimerization, suggesting that Jα

plays a strong role in thermal caging (**Figure 4D-F, Movie S4**), in addition to its established role in optical caging. Similar effects of DUF and Jα were obtained with another membrane-binding construct, AH1-DUF-STIM1 (**Figure S12A-C**).

To test if temperature sensing is intrinsic to the protein, we performed structural assays on a purified MBP-Jα-AH1-DUF fragment, with MBP added to increase solubility *in vitro*. Limited trypsin proteolysis coupled with mass spectrometry showed differential cleavage patterns in the AH1 and DUF regions when incubated at 25°C vs 37°C. Notably the core of the DUF domain remained stable under both conditions **(Fig S13-14).** To further characterize temperature-dependent conformational changes within the MBP-Jα-AH1-DUF fragment**,** we subjected it to hydrogen-deuterium exchange coupled to mass spectrometry (HDX-MS), which measures conformational change by quantifying changes in solvent-accessibility of amino acids by their rate of deuterium incorporation when placed in deuterated water, D_2O (*36*). While HDX-MS showed no global changes in deuterium uptake performed at 25°C vs 37°C, consistent with the fragment retaining its overall stability, we observed substantial changes in uptake in discrete regions (**Figure 4G**). This included the 459-472 region which intriguingly showed *decreased* exchange at higher temperature, counter to expectations of *increased* exchange from the mechanism of the exchange reaction (*37*). Few mechanistic explanations can account for such a change, the most probable of which is a temperature-dependent increase in protein interactions in this region.

To search for residues involved in potential temperature-dependent intra-molecular contacts, we performed a multi-sequence alignment of the corresponding Jα-AH1-DUF region from 69 BcLOV4 homologues and examined the degree to which each amino acid co-varied with each other amino acid in the evolutionarily-related sequences (*38*). Remarkably, we found strong co-variation of amino acids in the 460 region with those near the 560 position (**Figure 4H**), the same regions that were independently identified by HDX-MS and limited proteolysis (**Figure 4G, S13-14**). The 460 region showed residues that were both highly conserved and highly variable (**Figure S15A**). The conserved amino acids were crucial to light response, since replacement of any of these conserved residues with alanine (Y460, L467, V469) resulted in proteins that could not respond to light even at low temperatures (**Figure S15B**). By contrast, mutation of the variable residues was not only well tolerated but could also tune the temperature-sensing properties of BcLOV4 (**Figure S15C)**. N466I lowered the temperature at which optogenetic responses could be observed, while N466A and N466M mutations allowed stronger BcLOV4 light responses at both high and low temperatures compared to the wt protein (**Figure S15C**). Notably, the I, M, and A substitutions are all found in BcLOV4 homologues, suggesting that their selection may be related to their functional effects on light- and temperature-sensing. To test the functional impact of potential interactions between the 460 and 560 regions, we investigated the co-evolved N466A/A561V mutation pair, which appeared in ~7% of our homolog dataset and 63% of N466A-containing sequences. Remarkably, this double mutant synergistically increased membrane localization in response to light and provided a substantial increase in activation duration at 37°C, whereas the individual mutations showed only mild or no effects on kinetics in isolation (**Figure 4I-J, S16**). When expressed in HEK 293T cells, the double mutant could be stimulated to reside on the membrane for over 18 hrs, a substantial increase over the wild-type protein, which could only be maintained at the membrane for 1-2 hours under even optimal conditions (**Figure 4I-J, S1B, S16C, Movie S5**)(*18*). This double-mutant also increased the duration and amplitude of an established BcLOV-based optogenetic probe of Ras/Erk signaling in a separate cell line (**Figure S17**) (*18*).

Notably, extended membrane localization of the double mutant was achieved under only intermediate levels of light stimulation (2% duty cycle, 12 mw/cm^2) at which activation of the wild-type BcLOV4 was minimal. Higher light levels (20% duty cycle) led to a higher initial magnitude of stimulation but subsequent membrane dissociation after several (~10) hours. This paradoxical behavior is captured by our model and is further evidence of an additional, irreversible inactive state that forms as a function of light, although the molecular nature of this state remains unclear (**Figure S1, 4I-J, S18, Movie S6**)(*18*).

Finally, we asked whether the thermo-sensitivity of the DUF domain could be harnessed to engineer thermal control over unrelated proteins, analogous to how optical control of photosensory domains has enabled modular optogenetic control over numerous and diverse targets (*27*). We thus fused DUF to Cry2$_{olig}$, a variant of Cry2 that clusters robustly at both low and high temperatures (**Figure 4K-L**). Remarkably, while DUF-Cry2$_{olig}$ clustered at 25C, clustering was suppressed at 37C. Thus, the temperature-dependent molecular changes in DUF can be harnessed and applied outside the context of BcLOV4 in a modular fashion.

Discussion

Light-induced pulsatory activation of BcLOV4 is generated by an intramolecular incoherent feed-forward circuit, demonstrating that individual proteins are capable of dynamic signal processing in the absence of larger networks. We also find that these response dynamics are tuned not only by an environmental cue—temperature—but also through evolution, suggesting a functional role for this step-to-pulse response.

The BcLOV4 IFFL is implemented by separate light- and temperature-sensing domains through competitive caging of an “activation” fragment (**Figure 4M**). Although it was initially proposed that LOV-Jα undocking uncages the AH1 binding region (*17*), our present work instead suggests that Jα undocking exposes charged residues that stimulate higher-order self-assembly, which causes membrane translocation through increased avidity of the AH1 region. At the same time, once undocked from LOV, the Jα-AH1 region can be caged by the C-terminal DUF domain at a rate that increases with temperature, thereby reducing clustering and membrane binding and completing incoherent regulation. Modeling the equilibria of these dark and light states captured the key dynamic features of BcLOV4, successfully predicted counterintuitive aspects of BcLOV4 regulation, and provided a mechanistic explanation for the observed reciprocal regulation of the LS and TI states in response to either light or temperature.

The domain-level IFFL also predicted a temperature-sensitive auto-inhibition, which we found to be mediated by DUF. While HDX-MS revealed regions in DUF that underwent conformational changes in response to temperature, future structural assays will be required to uncover the precise molecular contacts that mediate temperature sensing. These mechanistic details will allow us to tune and optimize single-component BcLOV-based optogenetic tools for use in mammalian cells by eliminating or further reducing its auto-inactivation after stimulation (**Figure S17**). More broadly, DUF temperature-sensing itself can be harnessed for temperature-controllable probes of living cells and organisms (**Figure 4K-L**) (*10*). While we previously showed this could be achieved in a point-mutant of BcLOV4 (called Melt (*10*)), we now show that the compact DUF domain could itself be harnessed for such applications (**Figure 4M)**. Understanding mechanisms of DUF thermo-sensing will allow tuning of its thermal switch point for such thermogenetic probes.

Deeper mechanistic studies may also reveal important principles by which proteins can trigger productive conformational changes in response to small changes in temperature.

Why does BcLOV4 generate pulses? BcLOV4 originates from *Botrytis cinerea*, a fungal pathogen of plants including grapes and strawberries. Perhaps a pulsed vs sustained response allows the host to distinguish the seasons, times of day, or levels of sun exposure to ensure optimal infection and fitness. While a functional role remains speculative, step-to-pulse dynamics are routinely observed across biological networks and have important consequences, for example in mitogenic regulation (*39*), stress adaptation (*5*, *8*, *40*), and gradient sensing (*11*). In these cases, however, pulse generation emerges from the collective action of protein networks, whereas BcLOV4 achieves this behavior on a smaller scale through networks of its domains. The capacity for dynamic encoding by a protein provides a blueprint for engineering more sophisticated, responsive, and compact biological systems.

Acknowledgements

The authors thank: Andreas Möglich and Brian Chow for helpful discussion on mechanisms of LOV domain photocycles; Wendell Lim for discussions on protein modularity and computation; Yuzhi Gao for help with cell sorting; Rinat Abzalimov for assisting peptide mass spectrometry; and James Siclari for helpful discussions of thermosensing in multiple protein systems. This work was supported by funding from the National Institutes of Health (R35GM138211 for L.J.B., R01 GM106239 for K.H.G.), the National Science Foundation (CAREER 2145699 to L.J.B.), and the Penn Center for Precision Engineering for Health (CPE4H Pilot grant to L.J.B.). Cell sorting was performed on a BD FACSAria Fusion that was obtained through NIH S10 1S10OD026986.

Contributions

Z.H., K.H.G, and L.J.B. conceived the study. Z.H. proposed the IFFL model and performed all the live cell imaging and simulations. M.F. purified the BcLOV4 fragment and performed and analyzed limited proteolysis and HDX-MS. W.B. characterized membrane association of BcLOV4-STIM1. L.J.B. and K.H.G supervised the work. Z.H. and L.J.B. wrote the manuscript and made figures, with editing from all authors.

Methods and materials

Plasmid constructs

BcLOV4 and SOScat genes were obtained from previous work (*18*). FTH1 was sourced from pCMV-SPORT6_FTH1, obtained from the High-Throughput Screening (HTS) Core at Penn Medicine. Cry2 (only the PHR domain was used in this study) sequence was obtained from previous work (*30*). The point mutations were introduced by using primers with altered sequences. DNA templates were amplified using Q5 hot start polymerase from NEB (M0493S), followed by HiFi assembly (NEB E2621S). The assembled products were transformed into chemically competent cells (NEB Turbo, C2984H) and subject to antibiotic selection.

Cell culture, transfection, viral packaging, and transduction

The LentiX-HEK 293T (TakaraBio, #632180) cells were cultured in DMEM with 10% fetal bovine serum (FBS) and 1% penicillin/streptomycin (P/S), while mouse fibroblast NIH 3T3 cells were cultured in DMEM with 10% calf serum (CS) and 1% penicillin/streptomycin (P/S). The cell culture incubators were set to 37C and 5% CO2 without further specification. Before optogenetic stimulation of Ras-Erk pathway in **Figure S17**, cells were serum starved overnight (5X 80% media change). The constructs were characterized in HEK293 cells using transient transfection without further specifications. The transfection was performed with calcium-phosphate precipitation. For long-term stimulation of BcLOV4 (**Figure 4K**) and optogenetic control of Ras-Erk signaling in 3T3 (**Figure S17**), cells were transduced with corresponding virus prepared by collecting the media from HEK cells 2 days after cotransfection of target plasmid, pCMVdR8.91, and pMD2.G (Addgene # 12259).The positive cells were sorted after expansion (AriaFusion).

Live cell microscopy and high-throughput profiling of light and temperature response

Cells were seeded into Cellvis 96 well plates (#P96-1.5P) coated with fibronectin (MilliporeSigma™ # FC010 diluted 100x in PBS) 24 hr (another 24 hr with transfection and expression) before imaging. Upon seeding, the cells were spun down onto the bottom of plates with 20g and 20 seconds. Live-cell imaging was then performed using a Nikon Ti2-E microscope with a Yokagawa CSU-W1 spinning disk, 405/488/561/640 nm laser lines, an sCMOS camera (Photometrics), and an environmental chamber with CO2 set to 5% and temperature set to 37C without further specifications (Okolabs). To characterize the temperature sensitivity of BcLOV4 variants, we used thremoplate to control the temperature in 96-well plates while imaging (*40*). The environmental chamber was set to 25C during thermoplate control. The thermoplate was allowed to warm up to the target temperature before inserting into the imaging plates. For characterizing light response under different duty cycles and temporal patterns, optoplate was used to deliver blue light from the top of the imaging plate and the confocal microscope was used for imaging from the bottom (*41*). For imaging with thermoplate and optoplate, 150 ul of culture media was added to each well and 100 ul PBS was added to the gaps of wells to prevent evaporation.

Immuno-fluorescence staining

For characterizing Ras-Erk signaling, we used Immuno-fluorescence staining of ppERK to characterize the result of optogenetic stimulation. Since BcLOV4 is temperature sensitive, and optoplate stimulation can generate heat, we used the thermoplate to maintain the temperature of each well at 37C (with incubator ambient temperature set to 32C) (*18*, *40*, *41*). The time course of signaling induction was obtained by starting the stimulation in different wells at different time points but with the same ending time (fixation). Upon completion of the experiment, the optoplate and the thermoplate were disassembled and cells were immediately fixed with 4%PFA (diluted from 16%) for 10 min in dark. Afterwards, the PFA-containing medium was aspirated and cells were permeabilized with 100 ul 0.5% Triton X-100 for 10 min (Sigma), followed by 100 ul ice-cold 100% methanol at -20°C for 10 min. Then, cells were blocked for 30 min at room temperature in Odyssey Blocking Buffer (LI-COR). Anti-ppErk (CST #4370, 1:400) primary antibody were then diluted in fresh blocking buffer. Blocking buffer was removed and cells were incubated in 50 ul primary antibody solutions for 2 hours. Cells were washed 5X with PBS with 0.1% Tween-20 (Sigma). Then the cells were incubated in secondary antibody (CST #SA5-10034, 1:500) together with DAPI (Molecular Probes, #D1306, 300 nM) for another hour followed by 5X wash with PBS with 0.1% Tween-20 (Sigma) (*41*). Then, the samples were imaged using a Nikon Ti2E epifluorescence microscope with DAPI/FITC/Texas Red/Cy5 filter cubes, a SOLA SEII 365 LED light source.

Protein purification

The Jα-AH1-DUF region of BcLOV4 (I356-F593) was amplified by PCR and cloned into a pMBP-6His-Parallel bacterial expression vector (*42*). The genetic construct was transformed into competent *E. coli* DH5α cells. All sequences were verified by Sanger sequencing. Recombinant proteins were expressed in *E. coli* BL21(DE3) cells (Stratagene). Cells were shaken (180 rpm) post-induction for 18–22 h at 18°C. Cells were harvested and resuspended in buffer containing 50 mM Tris [pH 8], 500 mM NaCl, 0.5% Triton X-100, 0.5 mM DTT, and lysed by sonication. Lysates were centrifuged at 34,571 xg, 4°C for 45 min. Supernatants were filtered through a 0.22 µm Corning syringe filter and bound to a 5 ml Ni^{2+} Sepharose affinity column (Cytiva). The MBP-6His tagged protein was washed with 10 column volumes of protein wash buffer (50 mM Tris [pH 8], 500 mM NaCl, 0.5 mM DTT, 10% glycerol, 50 mM imidazole) and eluted with protein wash buffer supplemented with 450 mM imidazole. Eluted proteins were further purified by size exclusion chromatography on a Superdex 200 16/40 (Cytiva) with SEC buffer containing 50 mM NaPi [pH 8], 150 mM NaCl, 3% glycerol, 0.5 mM DTT. Protein was concentrated using Amicron centrifugal concentrator with 50 kDa MWCO. Concentrations were determined from the theoretical absorption coefficient, ε_{280}= 90760 M^{-1} cm^{-1} for MBP-6His-Jα-AH1-DUF, calculated from the sequence using the ExPASy ProtParam server(*43*).

Limited proteolysis

Limited proteolysis reactions were performed with 50 µM MBP-6His-Jα-AH1-DUF in a buffer containing 50 mM NaPi [pH 8],150 mM NaCl, 3% glycerol, 0.5 mM DTT. Samples were equilibrated at 25°C and 37°C conditions pre-trypsinolysis. Trypsin was added in a 1:500 v/v ratio to MBP-6His-Jα-AH1-DUF at 25°C and 37°C. 40 µL aliquots of the reactions were quenched with 1 µL of PMSF quench solution (final concentration of 2 mM) at timepoints of 100, 500, 1000, 2000, 3600, 5000,

6000, and 7200 s. Quenched samples were subjected to SDS-PAGE analysis and visualized using Coomassie Blue stain. 3 µL of each terminated reaction was also analyzed for peptide population composition using HPLC-ESI MS/MS LC-MS/MS. The peptides were resolved using a C18 analytical column (Acclaim 300 C18, 3 µm, 2.1 x 1500 mm, Thermo Fisher Scientific) and analyzed on a Bruker maXis-II ETD ESI-QqTOF mass spectrometer. The resulting MS/MS fragments were analyzed using Bruker COMPASS DataAnalysis by deconvoluting the spectrum for specific peptide m/z signals. Peptide sequences were analyzed and identified by Peptide Analysis Worksheet Freeware Edition (PAWs, ProteoMetrics–freeware edition) and the ExPASy ProtParam server. Predicted masses were compared with experimentally generated masses to corroborate SDS-PAGE results.

HDX-MS

MBP-6His-Jα-AH1-DUF was purified as described above. The stock samples were concentrated to 40 µM and then microcentrifuged. The stock was equilibrated at 25°C and 37°C for 5 min. Deuterium exchange was initiated by adding 5 µL of protein sample to 70 µL of D_2O HDX buffer (50 mM NaPi [pD 7.6], 150 mM NaCl, 0.5 mM DTT, 3% glycerol, 99.9% D_2O) and allowed to proceed for 100, 1000, 3600 and 6000 s at 25°C and 37°C. At the end of each reaction time point, the reaction mix was quenched with 75 µL ice-cold quench buffer (3 M GdHCl, 3% acetonitrile, 0.8% formic acid) and kept on ice through all subsequent steps. Quenched protein samples were immediately injected over an Enzymate BEH Pepsin Column (Waters) to digest the protein, while also desalting the resulting peptides with a C18 Hypersil Gold 3 µm 10x1 mm trap column (Thermo Fisher Scientific). After 3 min post-injection, the peptides were resolved through a C18 analytical column (Hypersil Gold, 50 mm length,1 mm diameter, 1.9 µm particle size, Thermo Fisher Scientific) and injected into a Bruker maXis-II ETD ESI-QqTOF high-resolution mass spectrometer. All resulting data files were then imported into version 3.3 of the HDExaminer software (Trajan Automation) to calculate deuterium uptake profiles.

Prior to starting HDX experiments, “unlabeled” samples were run under identical conditions as HDX except the buffer was H_2O based to provide masses and retention times of undeuterated peptides as reference. The unlabeled run was performed with MS/MS fragmentation to identify peptides using Bruker COMPASS DataAnalysis 5.3 and BioTools 3.2 software. Every matched m/z and retention time pair was assigned to only one peptide sequence based on accurate mass and MS/MS measurements. This resulted in coverage of about 98% of the protein sequence. All peptide matches were manually confirmed after automatic assignment by HDExaminer. All HDX-MS experiments were conducted in duplicates.

Image analysis

The membrane binding was quantified using the ratio of the mean of membrane fluorescence and the mean of whole cell fluorescence. The cells were segmented with MorpholibJ, a plugin of imageJ (FIJI). The edge pixels of the segmented objects were defined as membranes. The measurements of pixel intensities were done with CellProfiler scripts. Then the output csv files were imported into customized R scripts with post-processing. For quantifications involving the comparison of dark state membrane association, the raw values are shown (e.g. **Figure 2K**), while for comparing

dynamic range of light response, the values normalized to dark state (the frame before light stimulation) are shown (e.g. **Figure 2H**).
The number and area of protein clusters within cells were quantified using a customized Matlab script (*33*). The algorithm first detects the center of clusters by the contrast with the surrounding area and then expands to the boundary of the clusters. The two parameters for center and edge detections were kept the same within the same experiment for comparisons between groups.
The ppERK staining quantification, the cells were segmented with DAPI (nucleus) and then a ring of 5 pixels surrounding the nucleus was taken for intensity measurements in both mCherry (expression of construct) and cy5 (ppERK staining) channels using CellProfiler. Then the output csv files were imported into customized R scripts with post-processing.

Multi-sequence alignment and co-evolution analysis

To search for BcLOV4 homologous that have altered temperature sensitivities, we blasted the sequence (BcLOV4 353-595) and took the top 69 hits. Then, multi-sequence alignment was performed using clustal-omega and visualized using Jalview. The sequence logo was generated using Seq2logo with logo type P-weighted Kullbuck Leibler (*44*). The same set of sequences were uploaded to Amoai for calculating the co-variation between every other amino acids (*38*)

Dynamic modeling

We modeled the state transitions of BcLOV4 with ordinary differential equations (ODEs). The kinetic model is illustrated in **Figure S1**. We used the following equations to model state transitions of BcLOV4:

$$d[LS]/dt = -k1 * [LS] + k2 * [AS] + s0 - d0*[LS] \quad (1)$$
$$d[AS]/dt = k1 * [LS] - k2 * [AS] + k3 * [TS] - k4 * [AS] + s0 - d0*[AS] \quad (2)$$
$$d[TS]/dt = -k3 * [TS] + k4 * [AS] + s0 - d0*[TS] - k5*[TS] \quad (3)$$
$$d[IS]/dt = k5*[TS] + s0 - d0*[IS] \quad (4)$$

To simulate the dynamics of the system upon temperature or light changes, initial distribution of the states are acquired through evolving a random distribution towards its equilibrium (or infinite time in ODEs) (**Figure 2B**). Then, the changes on light (k1 is increased to simulate illumination) or temperature (k3 is increased to simulate cooling) are imposed on the initial distribution and induce the transition between states. The energy terms are derived from the correlation between rate constants and activation energy given by:

$$k = Ae^{EA/RT} \quad (5)$$

E_A can be calculated as the difference between transition states and stable states (LS, AS, TI). Since the energy terms are relative, we set $E_{act} = 0$ unless specified and calculated other energy terms accordingly from the set of rate constants used in ODEs (**Figure 1H, J**). We also assume the transition states are kept constant under different environmental conditions. Please refer to

supplementary file 1 to see the analytical solutions of population distribution at equilibrium, the discussion on how light affects k5, and parameterization details.

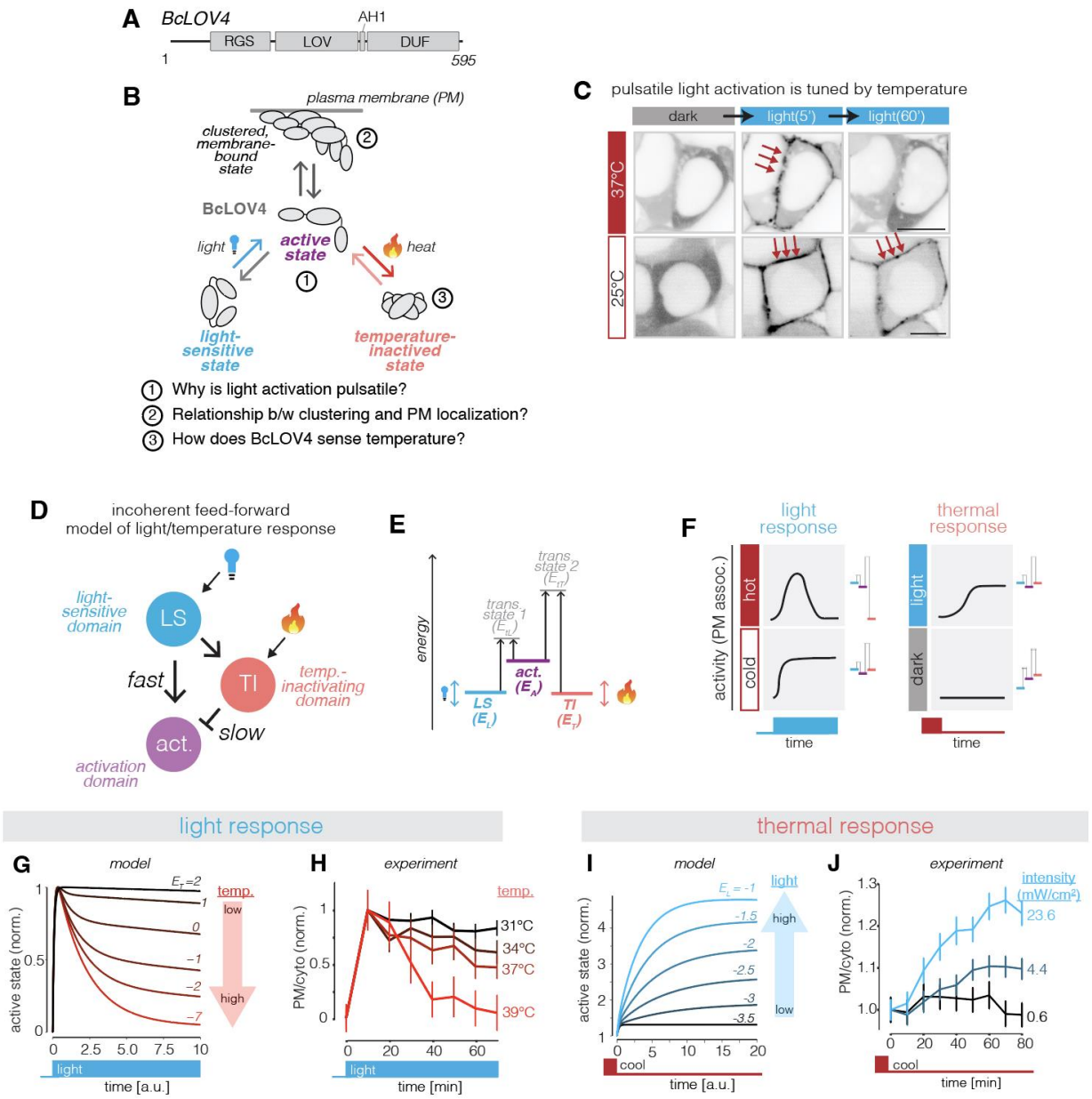

Fig 1. Incoherent feed-forward regulation (IFFR) explains dynamics of BcLOV4 response to light. (A) BcLOV4 domain arrangement. IDR, intrinsically disordered region. RGS, regulatory G-protein subunit. LOV, light-oxygen-voltage. AH1, amphipathic helix 1. DUF, domain of unknown function. **(B)** Hypothesized BcLOV4 state transitions with remaining mechanistic questions. **(C)** BcLOV4 light response is pulsatile, typical of IFFL regulation. Pulse kinetics can be adjusted by temperature. Also see **Movie S1**. Scale bar = 10 um. **(D)** A IFFL to describe domain interactions within BcLOV4 activation. Illumination activates the light sensitive (LS) domain to activate an activation domain (act.) but also licenses inhibition of this output through a temperature-inactivating(TI) domain on a slower time scale. **(E)** A thermodynamic model to describe the three hypothesized states that can implement IFFL regulation. Light and temperature stimulation are modeled by increasing or decreasing the energy levels of the LS or TI states, shifting the

distribution among the 3 states. **(F)** Predicted dynamics as a function of light and temperature. Energy levels indicate the final system state after stimulation. **(G,H)** Model and experiment of BcLOV4 light response under different temperatures. Cells were kept under target temperatures for 2 hours using the thermoPlate prior to illumination. Error bar represents +/- SEM of ~600 cells. **(I,J)** Model and experiment of BcLOV4 thermal response under different light conditions. The cells were pre-illuminated to populate the TI state (see Methods) and then cooled to 27°C under different intensities of light stimulation. Error bar represents +/- SEM of ~300 cells.

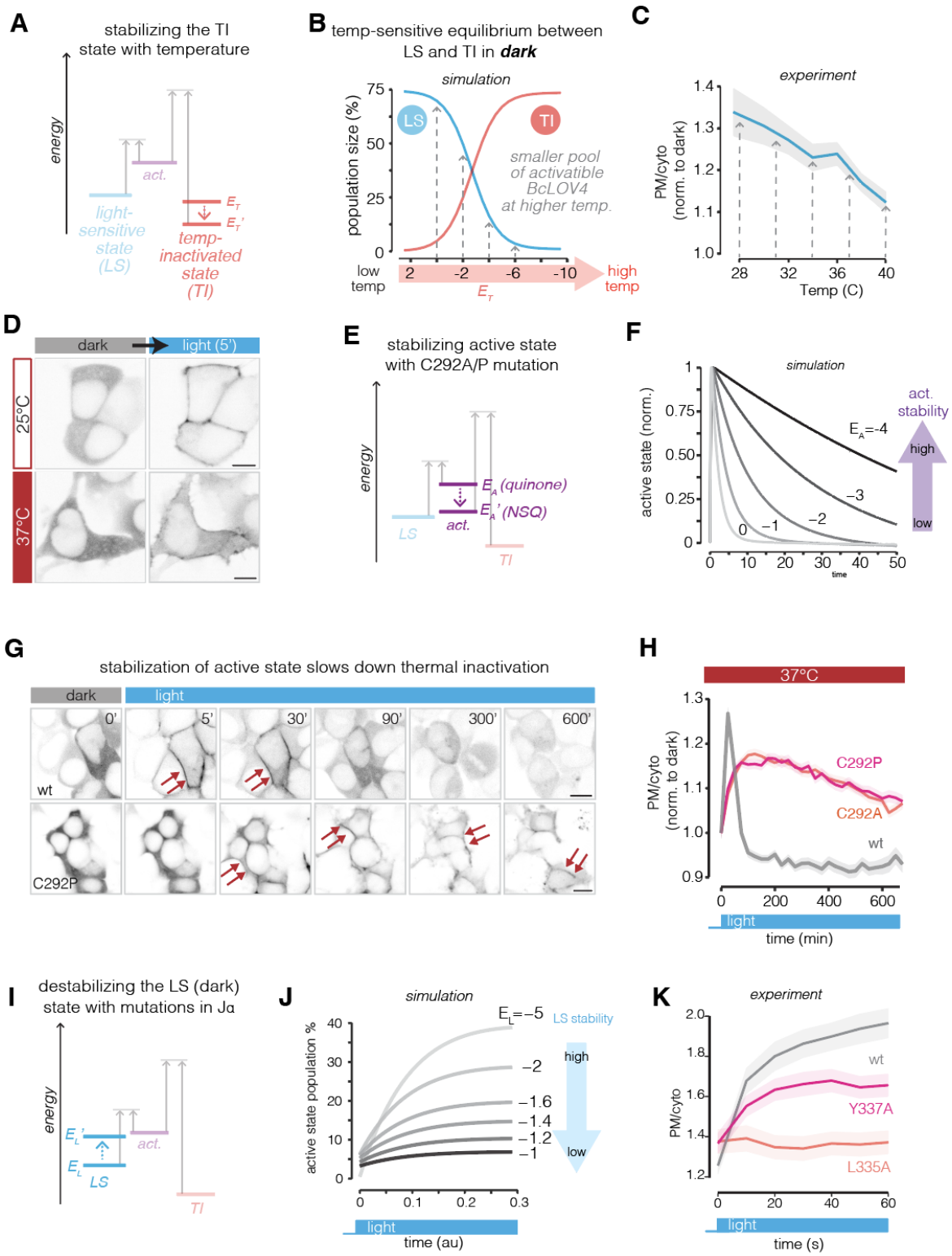
A
stabilizing the TI state with temperature
energy
act.
light-sensitive state (LS)
temp-inactivated state (TI)
B
temp-sensitive equilibrium between LS and TI in dark
simulation
population size (%)
LS
TI
smaller pool of activatible BcLOV4 at higher temp.
low temp
high temp
C
experiment
PM/cyto (norm. to dark)
Temp (C)
D
dark
light (5')
25°C
37°C
E
stabilizing active state with C292A/P mutation
energy
LS
act.
TI
F
simulation
active state (norm.)
act. stability
high
low
time
G
stabilization of active state slows down thermal inactivation
dark
light
0'
5'
30'
90'
300'
600'
wt
C292P
H
37°C
PM/cyto (norm. to dark)
C292P
C292A
wt
light
time (min)
I
destabilizing the LS (dark) state with mutations in Jα
energy
act.
LS
TI
J
simulation
active state population %
LS stability
high
low
light
time (au)
K
experiment
PM/cyto
wt
Y337A
L335A
light
time (s)

Fig 2. Validation of activation dynamics predicted by the thermodynamic IFFR model. (A) Stabilizing the temperature inactivated (TI) state with increased temperature should increase the amount of protein in the TI state even in the absence of light. **(B)** An increase in TI state population cannot be directly observed but can be inferred by a reciprocal change in the LS state, observed as the amount of protein that translocates to the membrane within minutes of light stimulation. **(C)** Measuring LS population (magnitude of membrane translocation after 3.5 min of blue light) in HEK 293T cells as a function of temperature. Data represent mean +/- SEM of ~530 cells. **(D)** Representative images of **(C)**. **(E)** Stabilizing the active state (act.) by mutation of C292 to promote active-state formation of the stable neutral semiquinone (NSQ). **(F)** Simulation of light-activation shows slower inactivation with increased active-state stability. **(G,H)** Experimental validation of active-state mutants. BcLOV4 variants were illuminated at 37C with constant light using optoPlate LEDs. Data represent mean +/- SEM of ~300 cells. **(I,J)** Destabilizing the light-sensitive (LS) state is predicted to result in higher basal membrane binding in the dark but decreased maximal binding in the light. (**K**) Experimental validation in HEK 293Ts with LS-destabilized variants with point mutations that weaken LOV-Jα interaction. Data represent mean +/- SEM of ~60 cells. Scale bar = 10 µm.

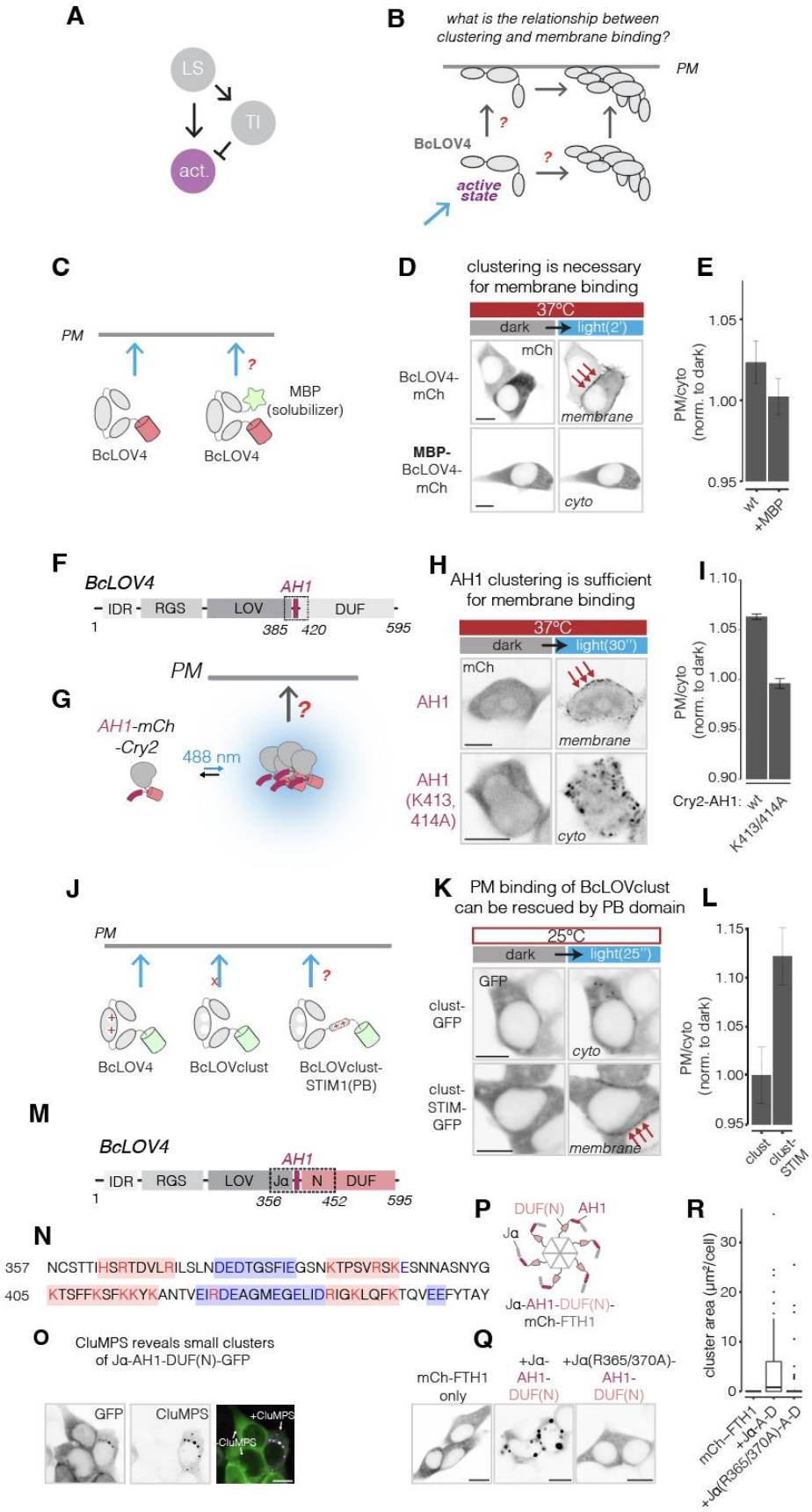
A
LS
TI
act.
B
what is the relationship between clustering and membrane binding?
PM
BcLOV4
active state
C
PM
MBP (solubilizer)
BcLOV4
BcLOV4
D
clustering is necessary for membrane binding
37°C
dark
light(2')
mCh
BcLOV4-mCh
membrane
MBP-BcLOV4-mCh
cyto
E
PM/cyto (norm. to dark)
1.05
1.00
0.95
wt
+MBP
F
BcLOV4
AH1
IDR
RGS
LOV
DUF
1
385
420
595
G
PM
AH1-mCh-Cry2
488 nm
H
AH1 clustering is sufficient for membrane binding
37°C
dark
light(30'')
mCh
AH1
membrane
AH1 (K413, 414A)
cyto
I
PM/cyto (norm. to dark)
1.10
1.05
1.00
0.95
0.90
Cry2-AH1:
wt
K413/414A
J
PM
BcLOV4
BcLOVclust
BcLOVclust-STIM1(PB)
K
PM binding of BcLOVclust can be rescued by PB domain
25°C
dark
light(25'')
GFP
clust-GFP
cyto
clust-STIM-GFP
membrane
L
PM/cyto (norm. to dark)
1.15
1.10
1.05
1.00
0.95
clust
clust-STIM
M
BcLOV4
AH1
IDR
RGS
LOV
Jα
N
DUF
1
356
452
595
N
357 NCSTTIHSRTDVLRILSLNDEDTGSFIEGSNKTPSVRSKESNNASNYG
405 KTSFFKSFKKYKANTVEIRDEAGMEGELIDRIGKLQFKTQVEEFYTAY
P
DUF(N)
AH1
Jα
Jα-AH1-DUF(N)-mCh-FTH1
R
cluster area (μm²/cell)
30
20
10
0
mCh-FTH1
+Jα-A-D
+Jα(R365/370A)-A-D
O
CluMPS reveals small clusters of Jα-AH1-DUF(N)-GFP
GFP
CluMPS
+CluMPS
-CluMPS
Q
mCh-FTH1 only
+Jα-AH1-DUF(N)
+Jα(R365/370A)-AH1-DUF(N)

615

Fig 3. Clustering drives membrane binding of BcLOV4. (A) Investigating mechanisms of the BcLOV4 active state. **(B)** Understanding the order and causality between protein clustering and membrane binding. **(C)** Testing necessity of clustering on translocation by fusion of a solubilizing MBP tag that suppresses protein assembly. **(D)** Light-induced membrane binding in HEK 293T cells after 2 min of stimulation. See **Fig S8** for further temperature conditions. **(E)** Quantification of **(D)**. Data represent mean +/- SEM of ~70 cells in each group. **(F,G)** Testing sufficiency of clustering of the AH1 region for membrane translocation. An extended AH1 fragment (385-420) was fused with Cry2, and protein localization was measured after light-induced clustering. **(H)** Protein localization in HEK 293T cells after 30s of light stimulation. Data show construct from **(G)** and a variant where key membrane-binding lysines were mutated to alanines. **(I)** Quantification of **(H)**. Data represent mean +/- SEM of ~800 cells. **(J)** Testing whether clustering of BcLOV is sufficient to drive weak polybasic domain (STIM1) to the membrane. **(K)** Comparing light-induced localization of BcLOVclust or BcLOVclust-STIM inHEK 293T cells. **(L)** Quantification of **(K)**. Data represent mean +/- SEM of ~130 cells in each group. **(M,N)** Patches of charged amino acids are found in the Jα-AH1-DUF(N) region (a.a. 356-452) after LOV domain. Red = positive charge, blue = negative charge. **(O)** Jα-AH1-DUF(N)-GFP appears diffuse in HEK 293T cells but triggers condensation when coexpressed with a CluMPS reporter, indicating the capacity of Jα-AH1-DUF(N) to form submicroscopic clusters. **(P)** Fusion of Jα-AH1-DUF(N) to a 24-meric FTH1 to test the clustering potential of this region. **(Q)** Jα-AH1-DUF(N)-mCh-FTH1 form large condensates in HEK 293T cells, and condensates depend on Jα and two arginine residues therein. Scale bar = 10 μm. **(R)** Quantification of **(Q)** (~30 cells per group).

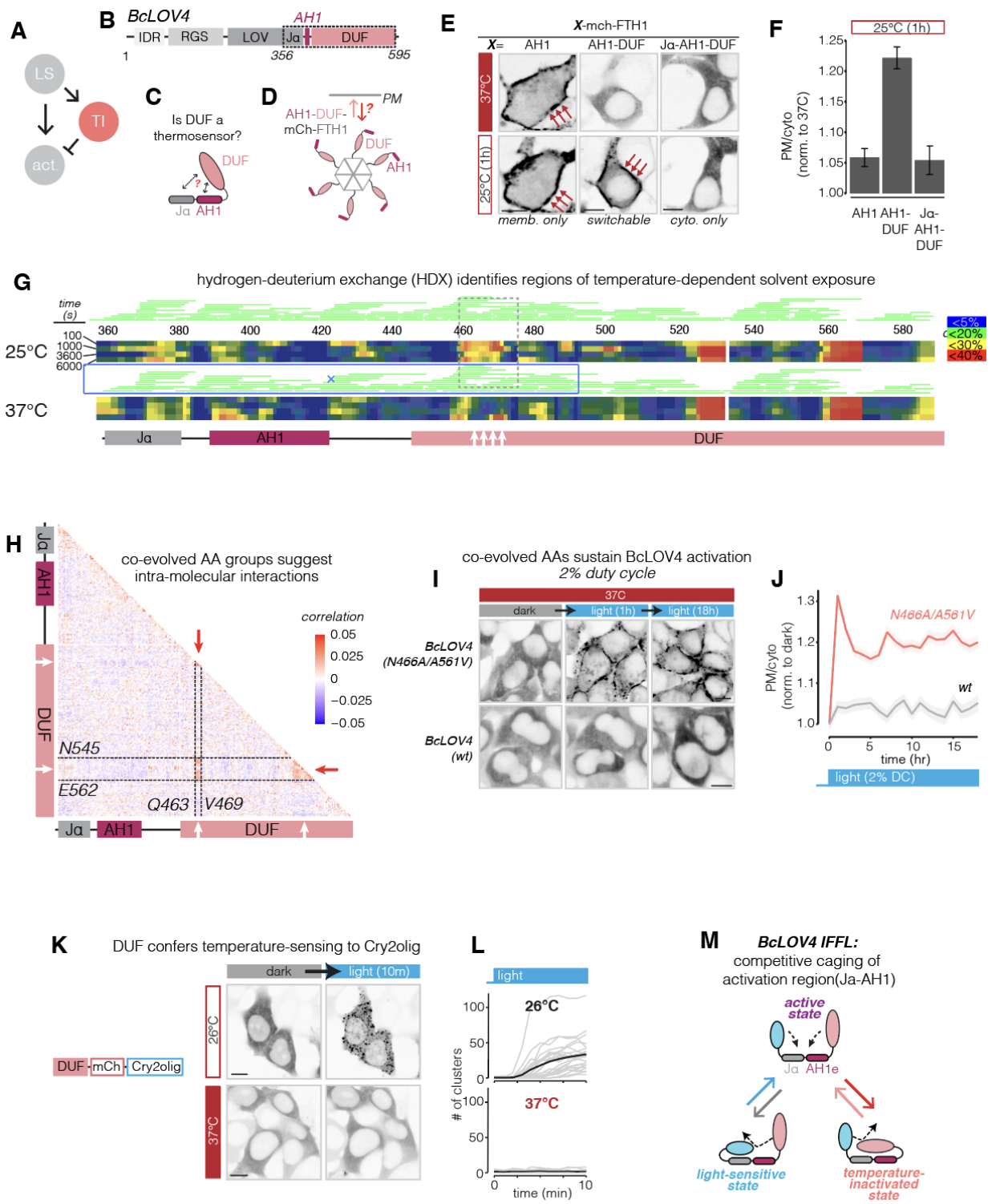

Fig 4. The DUF domain senses temperature and modulates IFFR kinetics. (A) Characterizing the mechanisms of the temperature-inactivated state. **(B,C)** The Jα-AH1-DUF fragment (a.a. 356-595) was investigated as a thermosensitive domain. **(D)** Membrane binding of FTH1 fused to Jα-AH1-DUF or truncations thereof was assessed at different temperatures. **(E)** Fusion to AH1 alone

(a.a. 385-420) yielded membrane binding at high and low temperatures; addition of the downstream DUF domain (AH1-DUF, a.a. 385-595) resulted in a switchable protein; further addition of an N-terminal Jα helix (Jα-AH1-DUF, 356-595) resulted in temperature-insensitive cytoplasmic localization. Also see **Movie S4**. Experiment performed in HEK 293T cells. Scale bar = 10 µm. **(F)** Quantification of **(E)**, showing ratio of membrane localization in the cold state to localization in the hot state. Data represent mean +/- SEM of ~700 cells. **(G)** Hydrogen deuterium exchange mass spectrometry (HDX-MS) showed temperature dependent conformational changes in the purified Jα-AH1-DUF (356-595) fragment. L456-G475 region (highlighted) showed marked temperature induced decrease in deuterium uptake at 37°C compared to 25°C. Time for deuterium exchange is shown on the left. Deuteration level is shown by the heat map. The unique peptides identified by mass spectrometry are indicated by green lines above the heatmap. **(H)** Covariation analysis revealed fragments of DUF that changed in concert through evolution, suggesting functional interactions. Color scale indicates likelihood (arbitrary unit) of an amino acid pair co-vary in the identified BcLOV4 homologs. Arrows and dashed lines highlight the regions with significantly higher confidence of co-evolution over surrounding regions. **(I)** The N466A/A561V double mutant can reside on PM for more than 18 hours after light stimulation in stably-expressing HEK 293T cells under low/intermediate light stimulation where wt BcLOV4 shows minimal activation. Also see **Movie S5**. Scale bar = 10 µm. **(J)** Quantitation of **(I)**. Data represent mean +/- SEM of ~280 cells. (**K**) Harnessing DUF for modular thermal control of unrelated proteins (full data see **Figure S19, Movie S7**). A DUF-Cry2olig fusion was tested for clustering propensity under different temperatures (pre-incubation for 2 hours). Scale bar = 10 µm. (**L**) Quantification of (**K**). Grey traces represent single cells, with black traces as average of them. 20-30 cells were quantified for each condition. **(M)** Model for the mechanism of the domain-level IFFL, which is implemented by competitive caging of the activation fragment (Jα-AH1) by both the light-sensing and temperature-sensing domains. In the LS state, Jα is caged by the LOV domain, and caging is released by light stimulation. Exposure of this region promotes clustering and subsequent membrane binding but also allows accessibility for thermal caging by the DUF domain, which occurs on slower timescales than light uncaging. On a slower time scale, TI domain binds Jα-AH1 to complete self-inactivation.

Supplementary figures

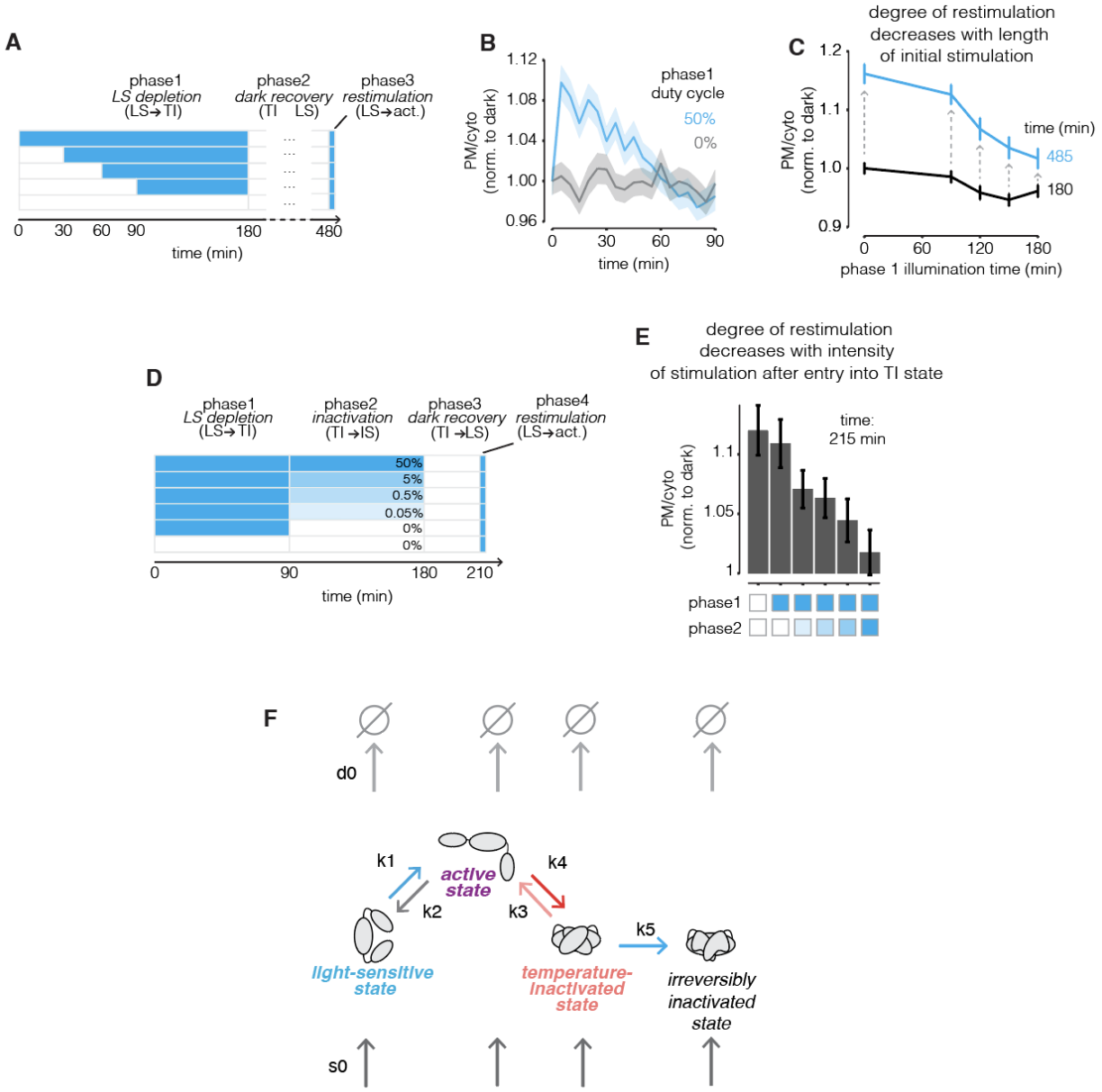

Fig S1. Kinetic model for BcLOV4 state transitions. (A) Protocol for testing the impact of length of light stimulation on the loss of reversibility of BcLOV4. In phase 1, HEK 293T cells (same for all panels in **Fig S1**) transfected with BcLOV4-mCh were stimulated with 0, 90, 120, 150, 180 min of light at 50% duty cycle (12 mW/cm^2, same for all panels in **Fig S1**), with light administration using an optoPlate. In phase 2, cells were incubated in the dark for 5 hours. In phase 3, cells were restimulated for 5 min to visualize the restored light-sensitive population. **(B)** Representative traces of membrane localization during phase 1 in **(A)**. BcLOV4 translocated to PM at the beginning of light stimulation and gradually dissociated from PM until its completion around 90 min. The data represent mean +/- SEM of ~550 cells. **(C)** The reversibility of BcLOV4 light response decreases with length of stimulation in phase 1. The black line indicates PM binding after phase 1 as a function

of illumination time, while the blue line indicates PM binding after phase 3. The difference between blue and black lines highlighted with gray arrows indicate the reversibility of light response. Data represent mean +/- SEM of ~300 cells on the blue line, ~680 cells on the black line. **(D)** Protocol for testing the impact of the light intensity on the loss of reversibility of BcLOV4. In phase 1, cells transfected with BcLOV4-mCh were stimulated with 50% duty cycle for 90 min to allow for full transition of the LS state to the TI state (as shown in **B**) or were kept in the dark. In phase 2, cells were stimulated for 90 additional mins using different duty cycles as indicated. In phase 3, the cells were incubated in the dark for 30 min. In phase 4, cells were restimulated for 5 min to visualize the degree of restoration of the LS population. **(E)** The PM binding after phase 4 restimulation between different stimulation patterns was compared. The duty cycles used in phase 1 and 2 are indicated by shading under the bars. Data represent mean +/- SEM of ~300 cells. **(F)** k1-k5 are rate constants for state transitions (k1 and k5 are functions of light, k3 is a function of temperature), s0 and d0 are rate constants for protein synthesis and degradation (same for each state for simplicity).

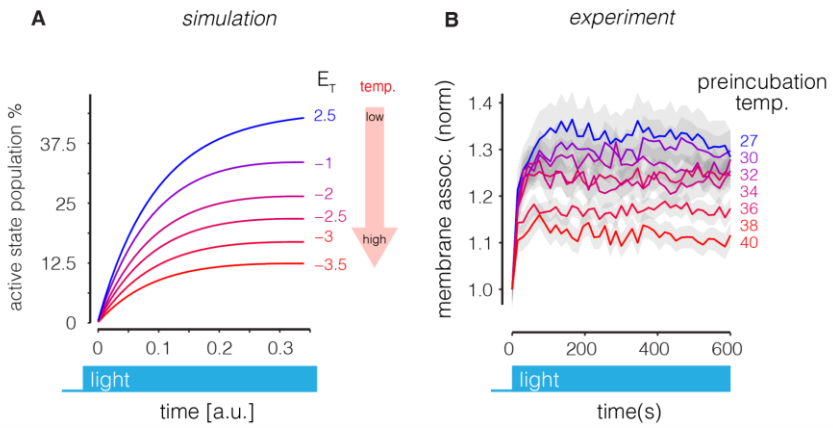

Fig S2. The effect of temperature on population distribution between states before light stimulation. (A) Light stimulation was simulated by increasing k1 after equilibrating populations under different temperatures (E_T). Simulation shows a lower amplitude of activation at higher temperatures. **(B)** Cells were incubated under different temperatures for two hours and then stimulated with blue light. The 210s time point was chosen to generate **Fig 2C**. Data show mean +/- SEM of ~530 cells.

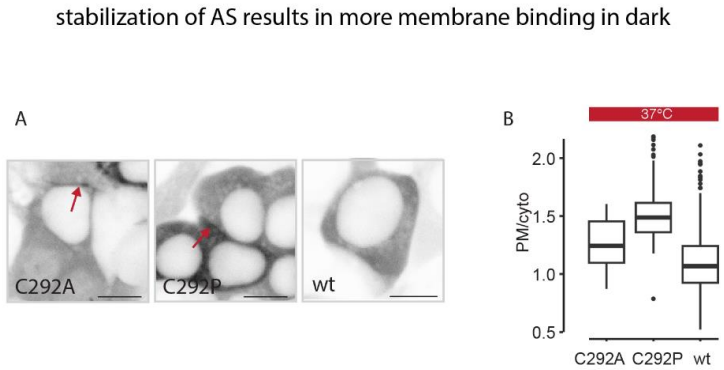

Fig S3. Mutations of the C292 stabilize the active state and result in elevated membrane binding in the dark. (A) HEK 293T cells were transfected with the indicated BcLOV4-mCh variants and were imaged after incubation at 37°C. Scale bar = 10 µm. **(B)** Quantification of (A). ~130 cells are quantified for each group.

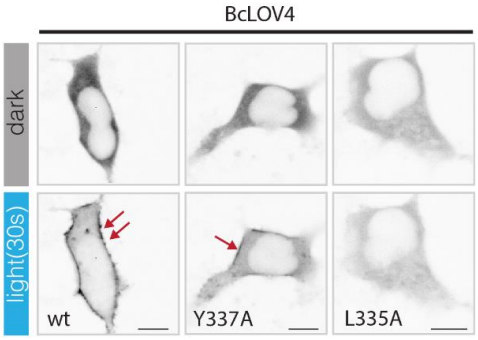

Fig S4. Destabilization of light-sensitive state results in a decrease in maximal activation. Representative images for **Fig 2K**. Scale bar = 10 µm.

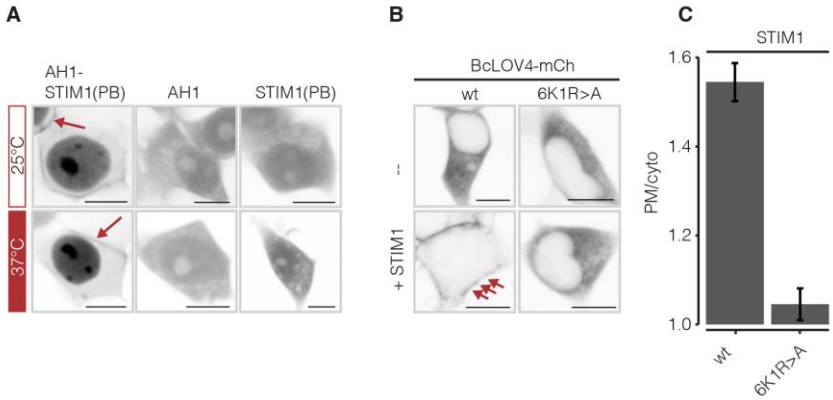

Fig S5. Evidence that AH1 is exposed in the dark. (A) AH1 binds the plasma membrane when fused with another weak membrane-binding domain from STIM1. **(B)** BcLOV4 binds PM when fused to STIM1 in the dark in an AH1-dependent manner. **Mutation of 6 lysines and 1 arginine in AH1** (6K1R, BcLOVclust) abrogates membrane binding, suggesting that these amino acids contribute to membrane binding in the dark and are thus exposed. **(C)** Quantification of **(B)**. 6K1R>A refers to mutation of K388, 395, 405, 410, 413, 414A, R393A, which are the positive charges important for PM binding (*20*). Data represent +/- SEM of ~70 cells. Scale bar = 10 µm.

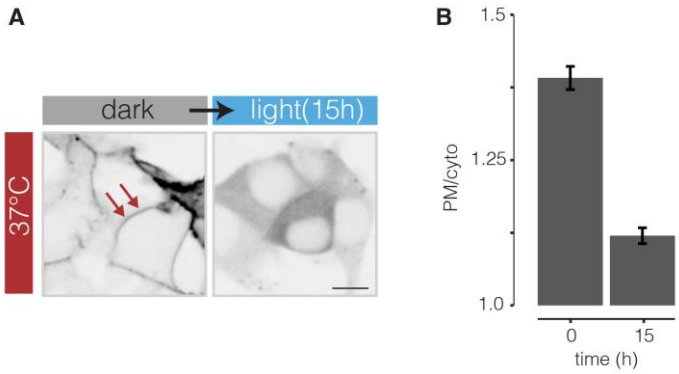

Fig S6. AH1 is occluded after long term light stimulation at 37°C. HEK 293 cells transfected with BcLOV4-STIM1 were cultured at 37°C and illuminated for 15 hrs using the optoPlate (5.9 mW/cm^2 and 50% duty cycle). Data represent mean +/- SEM of ~450 cells. Scale bar = 10 µm.

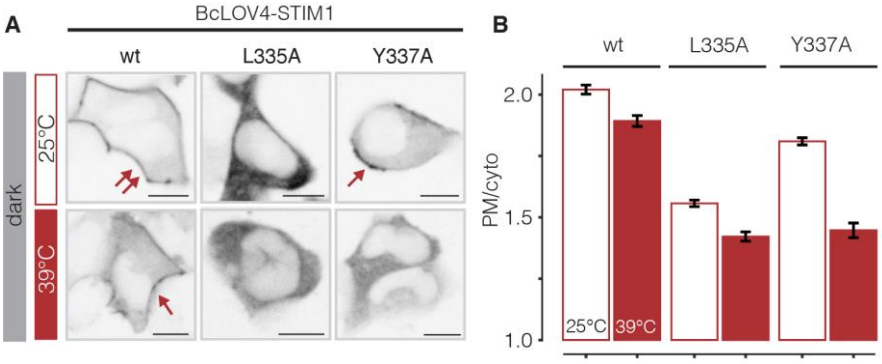

Fig S7. Destabilization of light-sensitive (LS) state reduces membrane-binding of BcLOV4-STIM1 in the dark. (A) Either L335A or Y337A weakening LOV core and Jα interactions was introduced to BcLOV4-STIM1. HEK 293T cells transfected with the indicated constructs were incubated at 25°C or 39°C for 2 hours before imaging. **(B)** Data represent mean +/- SEM of ~800 cells (25°C) and ~400 cells for (39°C). Scale bar = 10 µm.

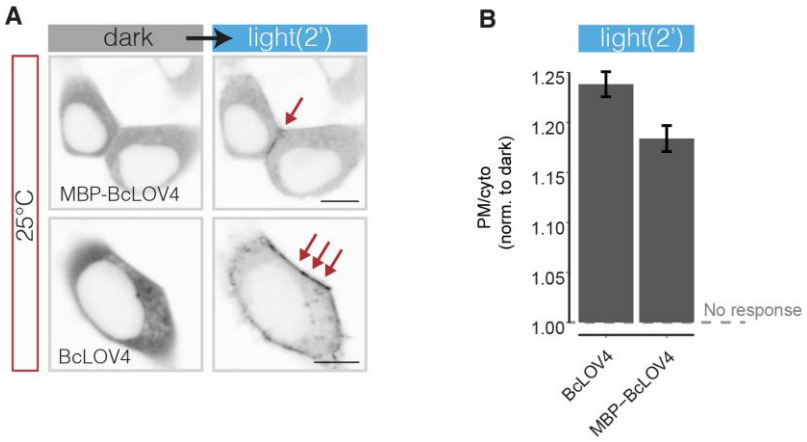

Fig S8. Fusion of MBP to BcLOV4 translocates to the membrane at 25°C but to a lesser degree than wt BcLOV4. Cells were incubated at 25°C for 2 hours before imaging. Data represent mean +/- SEM of ~70 cells. Scale bar = 10 µm.

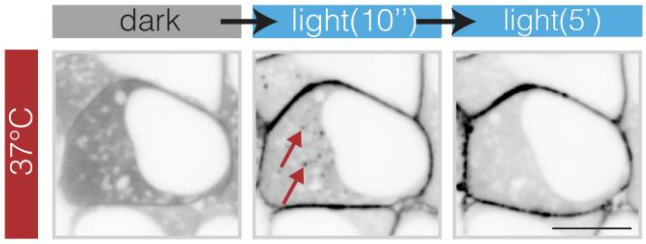

Fig S9. BcLOV4 transiently forms visible clusters in the cytoplasm within seconds of light stimulation. High-magnification confocal microscopy reveals the presence of transient clusters, which disappear likely due to translocation to the membrane. Scale bar = 10 µm. Also see also Movie S2.

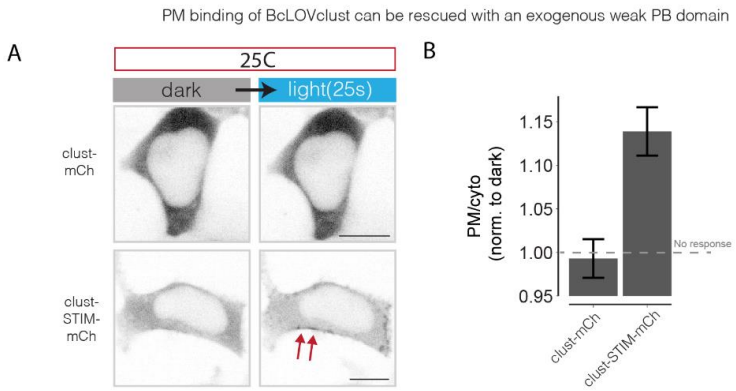

Fig S10. STIM1 fusion rescued membrane binding of BcLOVclust-mCh at 25°C. (A) HEK 293T cells expressing the indicated constructs were incubated at 25°C for 2 hours before imaging. Cells were illuminated for 25 seconds. **(B)** Quantification of **(A)**. Data represent mean +/- SEM of ~100 cells. Scale bar = 10 µm.

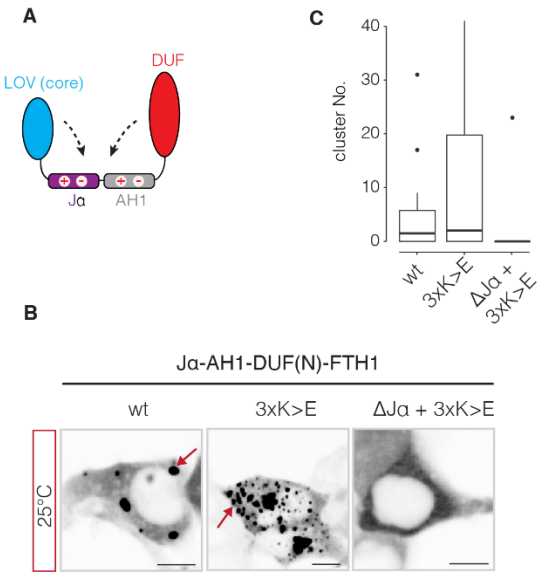

Fig S11. Jα and balanced charge distribution are crucial for BcLOV4 clustering at 25°C. (A) Jα-AH1-DUF(N) is the BcLOV4 fragment from amino acids 356 to 452, within which alternating positive and negative amino acid patches were found (**Figure 3N**). **(B)** HEK 293T cells were transfected with the indicated constructs and incubated at 25°C for one hour before imaging. 3K>E refers to introducing K to E mutations at K405, K410, and K414, which are important positions for membrane-binding that were identified previously (*20*). "ΔJα" refers to the wt fragment but excluding the Jα helix (a.a. 385-452). Scale bar = 10 µm. **(C)** Quantification of **(B)**. 28-61 cells were quantified for each group.

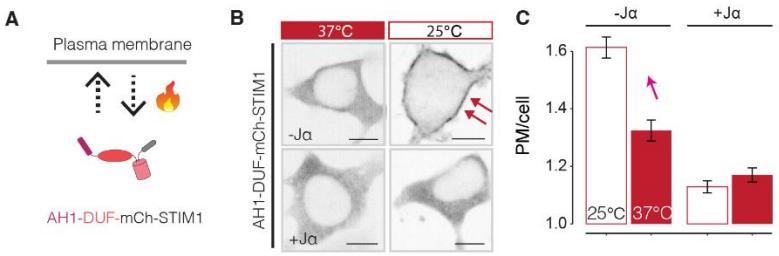

Fig S12. DUF domain shows temperature sensitivity across multiple systems. (A) In addition to FTH1 utilized in **Figure 4D-F**, AH1-DUF (385-595) was fused with STIM1 poly basic domain for testing temperature sensitivity. **(B)** HEK 293T cells were transfected with the indicated constructs with or without Jα (356-384) and imaged after pre-incubation at either 37°C or 25°C overnight. While the AH1-DUF fragment responds to temperature, addition of Jα suppresses switchability. Scale bar = 10 um. **(C)** Quantification of **(B)**. Data represent mean +/-SEM of ~300 cells.

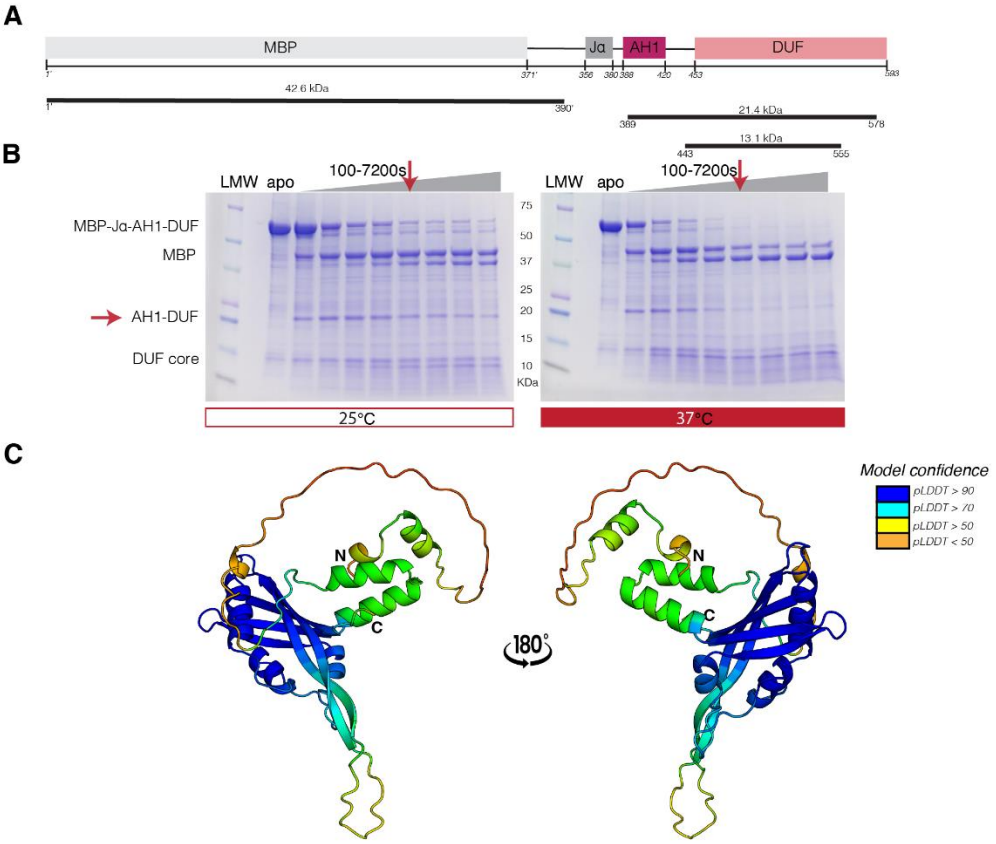

Fig S13. Limited proteolysis reveals thermostability and thermoswitchability of the AH1-DUF region of BcLOV4. (A) Domain schematic of MBP-Jα-AH1-DUF protein. Note that residues in the MBP and linker regions preceding Jα-AH1-DUF are designated differently (1’ - 403’) than those from Jα-AH1-DUF (numbered 356 - 593, as in full length BcLOV4). (B) SDS-PAGE gels show patterns of trypsin digestion of MBP-Jα-AH1-DUF at 25°C and 37°C over 7200 s. Cleavage of the soluble MBP tag from the MBP-Jα-AH1-DUF fusion is observed early under both conditions, with MBP staying thermostable under all conditions. AH1-DUF was moderately thermoresistant at 25°C, with some increased degradation at 37°C. A region predicted to be a thermostable part of the DUF domain was persistently observed at ~13.1 kDa. (C) AlphaFold3 model of Jα-AH1-DUF, colored by pLDDT confidence scores mapped onto structure.

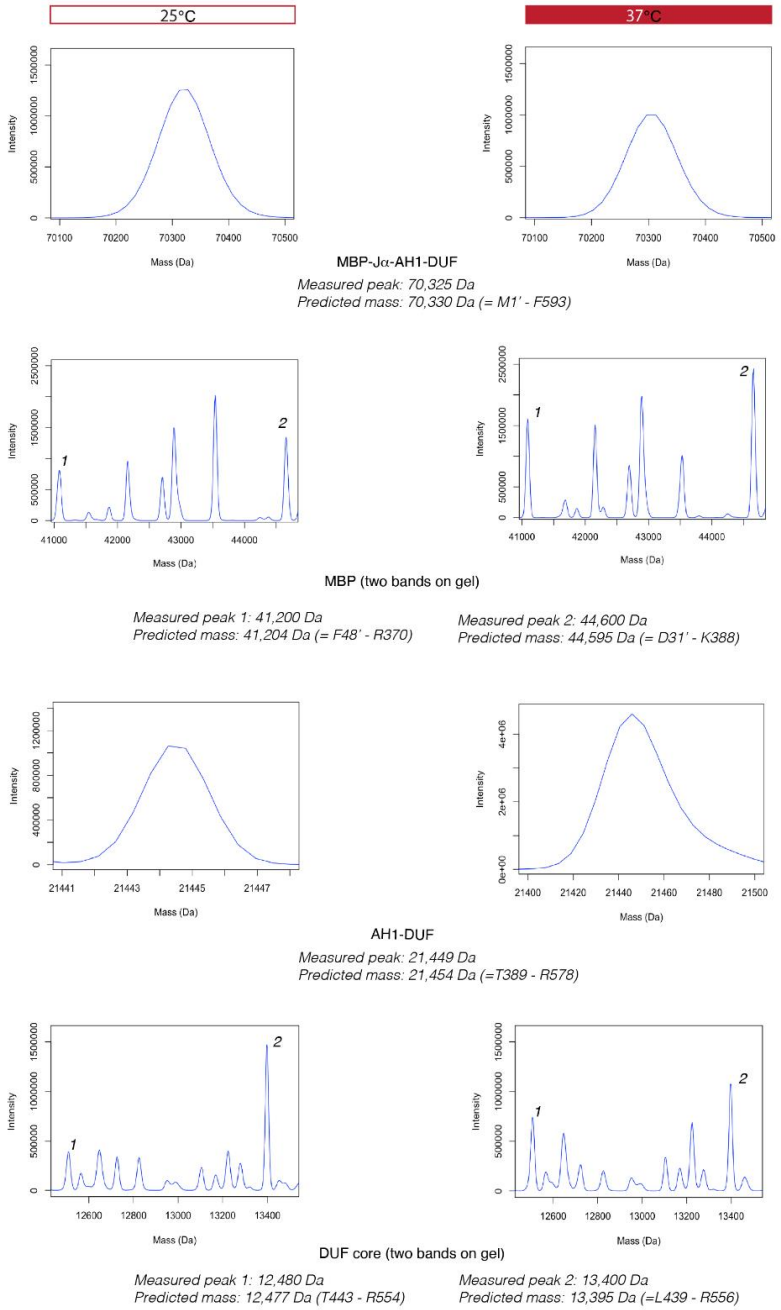

Fig S14. Mass spectrometry data used for identifying fragments in limited proteolysis experiments of MBP-Jα-AH1-DUF. Chromatograms depicting measured masses are shown for various bands that appear prominently in SDS PAGE gel. Note that residues in the MBP and linker regions preceding Jα-AH1-DUF are designated differently (1' - 403') than those from Jα-AH1-DUF (numbered 356 - 593, as in full length

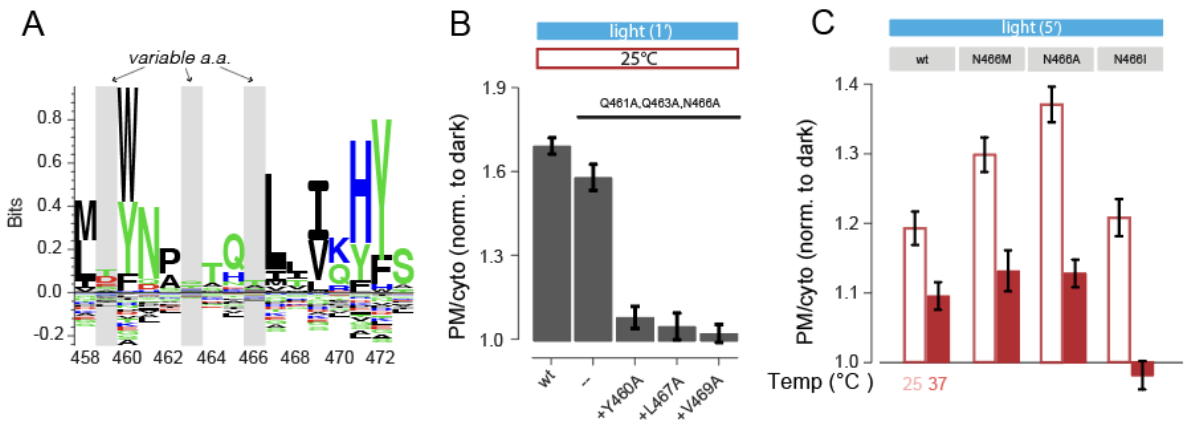

Fig S15. Evolutionarily varied amino acids modulate BcLOV4 temperature sensing. (A) Amino acid conservation of the BcLOV4(354-595) region among 69 homologues shows highly conserved and highly variable amino acids. **(B)** Mutations in conserved amino acids around position 465 resulted in poorly light responsive proteins. The degree of membrane binding after 1 minute of light stimulation was quantified. Whereas a triple mutation of non-conserved amino acids had little effect, additional mutation of any of three conserved amino acids substantially reduced light-dependent activation in HEK 293T cells. Cells were incubated under 25°C for 2 hours prior to stimulation. Data represent mean +/- SEM of ~150 cells. **(C)** N466 was replaced with amino acids found in BcLOV4 homologues (**Fig 4H**). Mutants were transfected into HEK 293T cells and were incubated under the specified temperatures for 2 hours prior to light stimulation. The identity of the amino acid mutation could either increase or decrease the magnitude of activation at high temperatures. Data represent mean +/- SEM of ~180 cells.

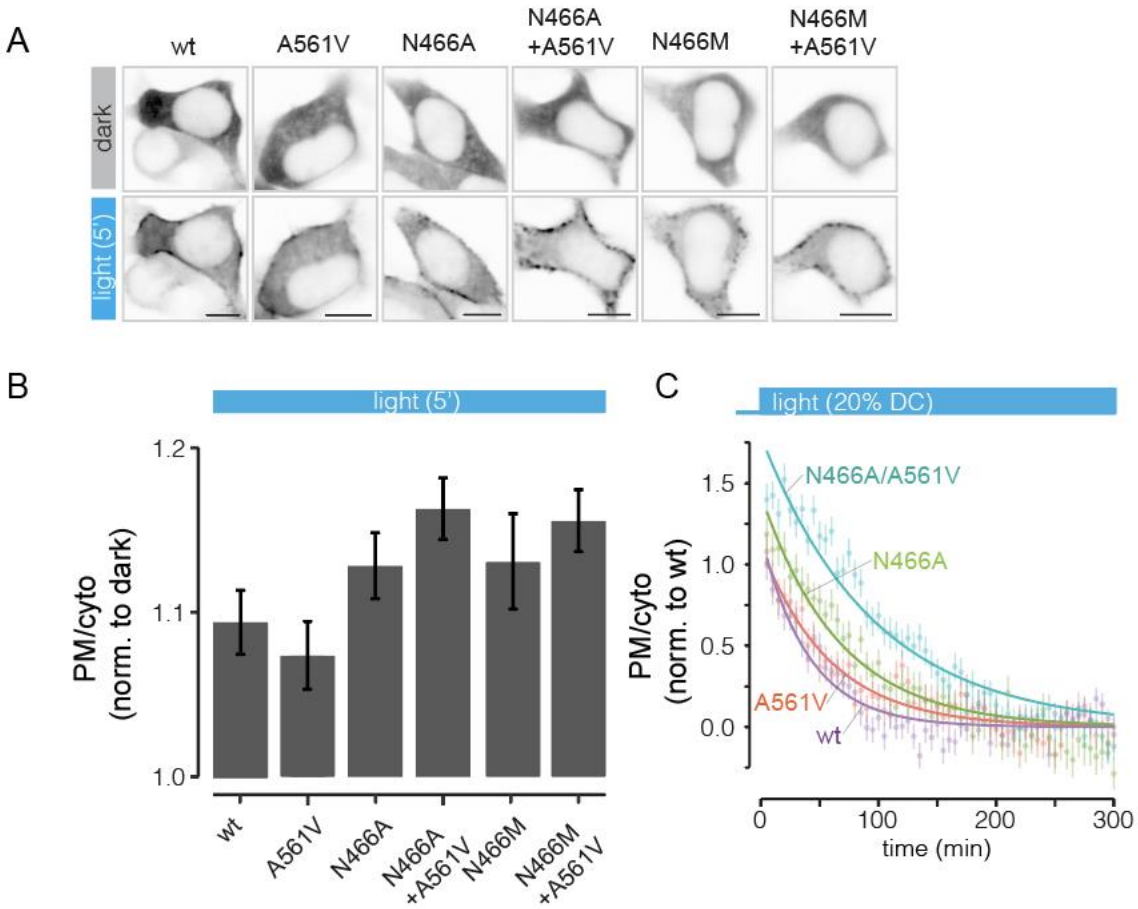

Fig S16. Synergistic enhancement of membrane binding by addition of A561V to N466 variants. Constructs were expressed in HEK 293T cells, which were incubated at 37°C after transfection. **(A)** Representative images of BcLOV4 variants light response. Scale bar = 10 µm. **(B)** Quantification of **(A)**. Data represent mean +/- SEM of ~220 cells. **(C)** Time course of long-term light stimulation of BcLOV4 variants with replacement of co-evolved amino acids from homologs. Data are normalized to the max and min of membrane translocation for the wt BcLOV4 protein. Light was delivered through optoplate with 20% duty cycle and 12 mW/cm^2. Data represent mean +/- SEM of ~250 cells.

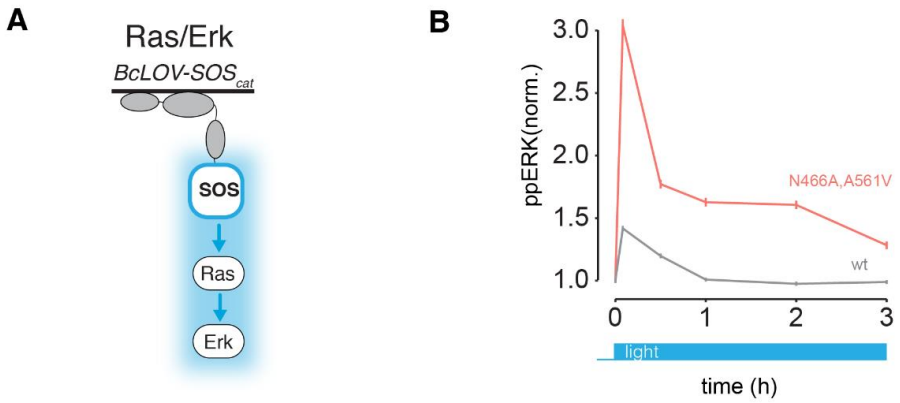

Fig S17. DUF domain mutants enhance the potency and thermostability of BcLOV4-based signaling probes. (A) Ras-Erk signaling can be controlled by translocation of the SOS catalytic domain to plasma membrane (BcLOV4-SOS_{cat}) (*18*). **(B)** NIH 3T3 cells stably expressing BcLOV4-mCh-SOS_{cat} (wt or N466A/A561V) were serum starved overnight and then stimulated with blue light (3.9 mW/cm^2, 30% duty cycle) at 37°C. Data show immunofluorescence for phospho-ERK (ppERK) as a marker of pathway activity. Data represent mean +/- SEM of ~4500 cells per data point. The double mutant allows more potent and durable stimulation of the pathway relative to wt BcLOV4.

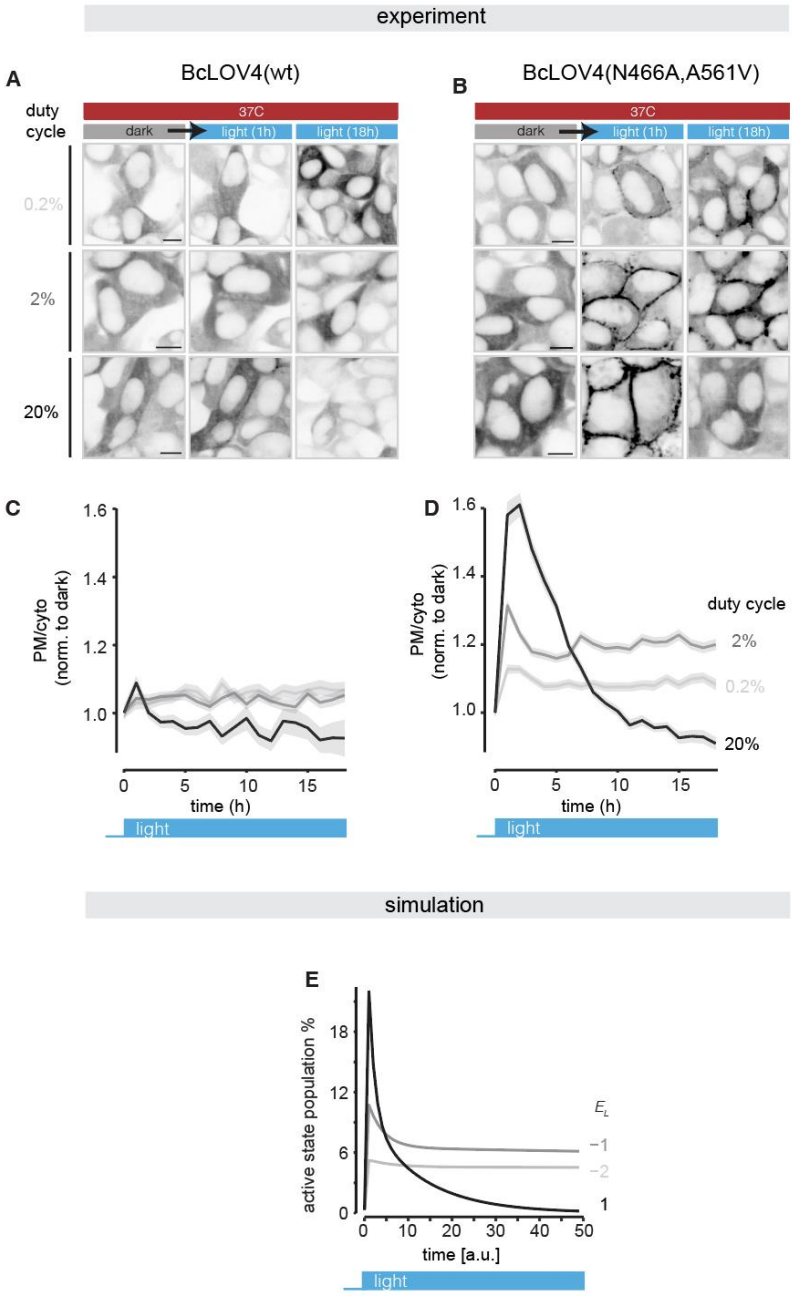

Fig S18. Stable long-term activation of the N466A/A561V double mutant occurs under only intermediate light stimulation. (A,B) HEK 293T cells stably expressing either wt BcLVO4 or the N466A/A561V double mutant and were illuminated at variable duty cycles over 18 hours using the optoPlate (see Methods for details). Cells were cultured under 37°C. Light intensity stimulation intensity was 12 mW/cm^2 and was applied at variable duty cycles. Scale bar = 10 µm. **(C,D)** Quantification of (**A,B**). The intersections between 20% duty cycle trace and others indicate a higher rate of entering irreversible state under higher duty cycles. Data indicate mean +/- SEM of ~ 280 cells. **(E)** The kinetic model (**Fig S1**) captures stable activation under intermediate stimulation but full decay under stronger stimulation, further supporting a light-dependent inactivation step.

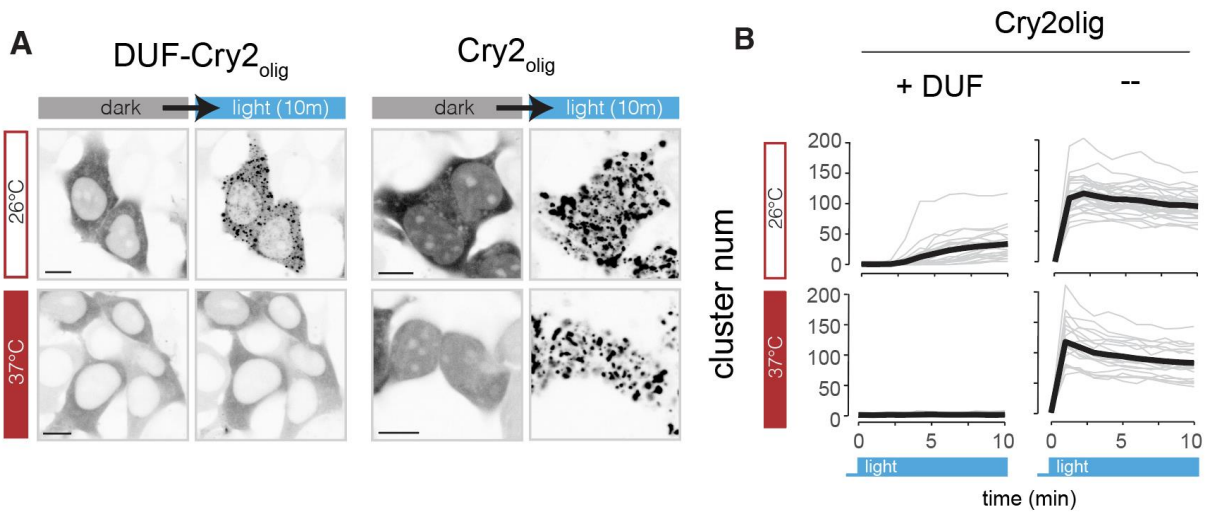

Fig S19. Modular thermal regulation of unrelated proteins with DUF. Part of data is shown in **Figure 4K-L. (A)** HEK 293T cells were transfected with either DUF-Cry2$_{olig}$ or Cry2$_{olig}$. Cells were stimulated with blue light under 37°C or 26°C (2 hours pre-incubation). Scale bar = 10 µm. (**B**) Quantification of (**A**). Cluster number in each cell is quantified under each of the four conditions. Grey traces represent single cells, with black traces show the mean. 20-30 cells were quantified for each condition.

Supplementary movies

Movie S1. **BcLOV4 light response is pulsatile, typical of IFFL regulation.** Pulse kinetics can be adjusted by temperature, with a faster self-inactivation rate at 37C than 25C. BcLOV4-mCh was expressed in HEK 293T cells. Scale bar = 10 um. Also see **Figure 1C**.

Movie S2. **BcLOV4 transiently forms visible clusters in the cytoplasm within seconds of light stimulation.** High-magnification confocal microscopy reveals the presence of transient clusters, which disappear likely due to translocation to the membrane. HEK 293T cells expressing BcLOV4-mCh were imaged at 37C. Scale bar = 10 µm. Also see **Figure S9**.

Movie S3. **Testing sufficiency of clustering of the AH1 region for membrane translocation.** Either an extended AH1 fragment (385-420) or a fragment with lysines (413 and 414) mutated to alanine was fused with Cry2, and protein localization was visualized after light stimulation. The proteins were expressed in HEK 293T cells. Scale bar = 10 um. Also see **Figure 3H**.

Movie S4. **Membrane binding of AH1-DUF is temperature switchable.** AH1-DUF(385-595) is fused with FTH1 and expressed in HEK 293T cells for testing its temperature sensitivity. The cells were cultured at 37C after transfection and cooled down to 25C for an hour during imaging and warmed back to 37C after that. Scale bar = 10 um. Also see **Figure 4E**.

Movie S5. **Naturally occurring mutations in the DUF domain substantially increase the amplitude and duration of light response at 37C.** The N466A/A561V double mutant can reside on PM for more than 18 hours after light stimulation in stably-expressing HEK 293T cells under 2% duty cycle light stimulation where wt BcLOV4 shows minimal activation. Scale bar = 10 um. Also see **Figure 4K**.

Movie S6. **Stable long-term activation of the N466A/A561V double mutant occurs under only intermediate light stimulation.** HEK 293T cells were transfected with wt BcLVO4 or the N466A/A561V double mutant and were illuminated at variable duty cycles over 18 hours using the optoPlate (see Methods for details). Cells were cultured under 37°C. Light intensity stimulation intensity was 12 mW/cm^2 and was applied at variable duty cycles. Scale bar = 10 µm. Also see **Figure S16**.

Movie S7. **Harnessing DUF for modular thermal control of Cry2 clustering.** A DUF-Cry2olig fusion was transfected in HEK 293T cells and tested for clustering propensity under different temperatures. Scale bar = 10 µm. Also see **Figure 4K, S19**.

References

1. W. A. Lim, The modular logic of signaling proteins: building allosteric switches from simple binding domains. *Curr. Opin. Struct. Biol.* **12**, 61–68 (2002).

2. J. E. Dueber, B. J. Yeh, K. Chak, W. A. Lim, Reprogramming Control of an Allosteric Signaling Switch Through Modular Recombination. *Science*, doi: 10.1126/science.1085945 (2003).

3. Y. L. Vishweshwaraiah, J. Chen, V. R. Chirasani, E. D. Tabdanov, N. V. Dokholyan, Two-input protein logic gate for computation in living cells. *Nat. Commun.* **12**, 6615 (2021).

4. Z. Chen, R. D. Kibler, A. Hunt, F. Busch, J. Pearl, M. Jia, Z. L. VanAernum, B. I. M. Wicky, G. Dods, H. Liao, M. S. Wilken, C. Ciarlo, S. Green, H. El-Samad, J. Stamatoyannopoulos, V. H. Wysocki, M. C. Jewett, S. E. Boyken, D. Baker, De novo design of protein logic gates. *Science* **368**, 78–84 (2020).

5. J. H. Levine, Y. Lin, M. B. Elowitz, Functional roles of pulsing in genetic circuits. *Science* **342**, 1193–1200 (2013).

6. W. Ma, A. Trusina, H. El-Samad, W. A. Lim, C. Tang, Defining network topologies that can achieve biochemical adaptation. *Cell* **138**, 760–773 (2009).

7. J. Schlessinger, Cell signaling by receptor tyrosine kinases. *Cell* **103**, 211–225 (2000).

8. D. Muzzey, C. A. Gómez-Uribe, J. T. Mettetal, A. van Oudenaarden, A systems-level analysis of perfect adaptation in yeast osmoregulation. *Cell* **138**, 160–171 (2009).

9. P. Klein, S. M. Kallenberger, H. Roth, K. Roth, T. B. N. Ly-Hartig, V. Magg, J. Aleš, S. R. Talemi, Y. Qiang, S. Wolf, O. Oleksiuk, R. Kurilov, B. Di Ventura, R. Bartenschlager, R. Eils, K. Rohr, F. A. Hamprecht, T. Höfer, O. T. Fackler, G. Stoecklin, A. Ruggieri, Temporal control of the integrated stress response by a stochastic molecular switch. *Sci Adv* **8**, eabk2022 (2022).

10. W. Benman, Z. Huang, P. Iyengar, D. Wilde, T. R. Mumford, L. J. Bugaj, A temperature-inducible protein module for control of mammalian cell fate, *Nat. Methods* (2025). https://doi.org/10.1038/s41592-024-02572-4.

11. N. Barkai, S. Leibler, Robustness in simple biochemical networks. *Nature* **387**, 913–917 (1997).

12. L. J. Bugaj, A. J. Sabnis, A. Mitchell, J. E. Garbarino, J. E. Toettcher, T. G. Bivona, W. A. Lim, Cancer mutations and targeted drugs can disrupt dynamic signal encoding by the Ras-Erk pathway. *Science* **361** (2018).

13. R. Milo, S. Shen-Orr, S. Itzkovitz, N. Kashtan, D. Chklovskii, U. Alon, Network motifs: simple building blocks of complex networks. *Science* **298**, 824–827 (2002).

14. A. Levchenko, P. A. Iglesias, Models of eukaryotic gradient sensing: Application to chemotaxis of amoebae and neutrophils. *Biophys. J.* **82**, 50–63 (2002).

15. L. Goentoro, O. Shoval, M. W. Kirschner, U. Alon, The incoherent feedforward loop can provide fold-change detection in gene regulation. *Mol. Cell* **36**, 894–899 (2009).

16. S. Mangan, S. Itzkovitz, A. Zaslaver, U. Alon, The incoherent feed-forward loop accelerates the response-time of the gal system of Escherichia coli. *J. Mol. Biol.* **356**, 1073–1081 (2006).

17. S. T. Glantz, E. E. Berlew, Z. Jaber, B. S. Schuster, K. H. Gardner, B. Y. Chow, Directly light-regulated binding of RGS-LOV photoreceptors to anionic membrane phospholipids. *Proc. Natl. Acad. Sci. U. S. A.* **115**, E7720–E7727 (2018).

18. W. Benman, E. E. Berlew, H. Deng, C. Parker, I. A. Kuznetsov, B. Lim, A. F. Siekmann, B. Y. Chow, L. J. Bugaj, Temperature-responsive optogenetic probes of cell signaling. *Nat. Chem. Biol.* **18**, 152–160 (2022).

19. A. A. Pal, W. Benman, T. R. Mumford, Z. Huang, B. Y. Chow, L. J. Bugaj, Optogenetic clustering and membrane translocation of the BcLOV4 photoreceptor. *Proc. Natl. Acad. Sci. U. S. A.* **120**, e2221615120 (2023).

20. Z. Huang Dennis, W. Benman, L. Dong, L. J. Bugaj, Rapid Optogenetic Clustering in the Cytoplasm with BcLOVclust. *J. Mol. Biol.* **436**, 168452 (2024).

21. S. Mangan, U. Alon, Structure and function of the feed-forward loop network motif. *Proc. Natl. Acad. Sci. U. S. A.* **100**, 11980–11985 (2003).

22. S. M. Harper, L. C. Neil, K. H. Gardner, Structural basis of a phototropin light switch. *Science* **301**, 1541–1544 (2003).

23. M. Salomon, J. M. Christie, E. Knieb, U. Lempert, W. R. Briggs, Photochemical and mutational analysis of the FMN-binding domains of the plant blue light receptor, phototropin. *Biochemistry* **39**, 9401–9410 (2000).

24. E. F. Yee, R. P. Diensthuber, A. T. Vaidya, P. P. Borbat, C. Engelhard, J. H. Freed, R. Bittl, A. Möglich, B. R. Crane, Signal transduction in light–oxygen–voltage receptors lacking the adduct-forming cysteine residue. *Nat. Commun.* **6**, 1–10 (2015).

25. R. F. Hayward, A. Rai, J. R. Lazzari-Dean, A. E. Y. Lefebvre, A. G. York, M. Ingaramo, Magnetic control of the brightness of fluorescent proteins. Zenodo [Preprint] (2024). https://doi.org/10.5281/ZENODO.8137174.

26. T. E. Swartz, S. B. Corchnoy, J. M. Christie, J. W. Lewis, I. Szundi, W. R. Briggs, R. A. Bogomolni, The photocycle of a flavin-binding domain of the blue light photoreceptor phototropin. *J. Biol. Chem.* **276**, 36493–36500 (2001).

27. A. Losi, K. H. Gardner, A. Möglich, Blue-light receptors for optogenetics. *Chem. Rev.* **118**, 10659–10709 (2018).

28. L. He, J. Jing, L. Zhu, P. Tan, G. Ma, Q. Zhang, N. T. Nguyen, J. Wang, Y. Zhou, Y. Huang, Optical control of membrane tethering and interorganellar communication at nanoscales. *Chem. Sci.* **8**, 5275–5281 (2017).

29. E. H. Brumbaugh-Reed, Y. Gao, K. Aoki, J. E. Toettcher, Rapid and reversible dissolution of biomolecular condensates using light-controlled recruitment of a solubility tag. *Nat. Commun.* **15**, 6717 (2024).

30. L. J. Bugaj, A. T. Choksi, C. K. Mesuda, R. S. Kane, D. V. Schaffer, Optogenetic protein clustering and signaling activation in mammalian cells. *Nat. Methods* **10**, 249–252 (2013).

31. T. J. Nott, E. Petsalaki, P. Farber, D. Jervis, E. Fussner, A. Plochowietz, T. D. Craggs, D. P. Bazett-Jones, T. Pawson, J. D. Forman-Kay, A. J. Baldwin, Phase transition of a disordered nuage protein generates environmentally responsive membraneless organelles. *Mol. Cell* **57**, 936–947 (2015).

32. W. Borcherds, A. Bremer, M. B. Borgia, T. Mittag, How do intrinsically disordered protein regions encode a driving force for liquid-liquid phase separation? *Curr. Opin. Struct. Biol.* **67**, 41–50 (2021).

33. T. R. Mumford, D. Rae, E. Brackhahn, A. Idris, D. Gonzalez-Martinez, A. A. Pal, M. C. Chung, J. Guan, E. Rhoades, L. J. Bugaj, Simple visualization of submicroscopic protein clusters with a phase-separation-based fluorescent reporter. *Cell Syst.* **15**, 166-179.e7 (2024).

34. D. Bracha, M. T. Walls, M.-T. Wei, L. Zhu, M. Kurian, J. L. Avalos, J. E. Toettcher, C. P. Brangwynne, Mapping Local and Global Liquid Phase Behavior in Living Cells Using Photo-Oligomerizable Seeds. *Cell* **176**, 407 (2019).

35. S. Boeynaems, E. Bogaert, D. Kovacs, A. Konijnenberg, E. Timmerman, A. Volkov, M. Guharoy, M. De Decker, T. Jaspers, V. H. Ryan, A. M. Janke, P. Baatsen, T. Vercruysse, R.-M. Kolaitis, D. Daelemans, J. P. Taylor, N. Kedersha, P. Anderson, F. Impens, F. Sobott, J. Schymkowitz, F. Rousseau, N. L. Fawzi, W. Robberecht, P. Van Damme, P. Tompa, L. Van Den Bosch, Phase separation of C9orf72 dipeptide repeats perturbs stress granule dynamics. *Mol. Cell* **65**, 1044-1055.e5 (2017).

36. Y. Hamuro, Interpretation of hydrogen/deuterium exchange mass spectrometry. *J. Am. Soc. Mass Spectrom.* **35**, 819–828 (2024).

37. Y. Bai, J. S. Milne, L. Mayne, S. W. Englander, Primary structure effects on peptide group hydrogen exchange. *Proteins* **17**, 75–86 (1993).

38. N. J. Cheung, A. T. John Peter, B. Kornmann, Leri: A web-server for identifying protein functional networks from evolutionary couplings. *Comput. Struct. Biotechnol. J.* **19**, 3556–3563 (2021).

39. A. Ram, D. Murphy, N. DeCuzzi, M. Patankar, J. Hu, M. Pargett, J. G. Albeck, A guide to ERK dynamics, part 2: downstream decoding. *Biochem. J.* **480**, 1909–1928 (2023).

40. W. Benman, P. Iyengar, T. R. Mumford, Z. Huang, M. Kapoor, G. Liu, L. J. Bugaj, Multiplexed dynamic control of temperature to probe and observe mammalian cells. *Cell Syst.* **16**, 101234 (2025).

41. L. J. Bugaj, W. A. Lim, High-throughput multicolor optogenetics in microwell plates. *Nat. Protoc.* **14**, 2205–2228 (2019).

42. P. Sheffield, S. Garrard, Z. Derewenda, Overcoming expression and purification problems of RhoGDI using a family of “parallel” expression vectors. *Protein Expr. Purif.* **15**, 34–39 (1999).

43. E. Gasteiger, C. Hoogland, A. Gattiker, S. Duvaud, M. R. Wilkins, R. D. Appel, A. Bairoch, *Protein Identification and Analysis Tools on the Expasy Server; (In) John M. Walker* (Humana Press, 2005).

44. M. C. F. Thomsen, M. Nielsen, Seq2Logo: a method for construction and visualization of amino acid binding motifs and sequence profiles including sequence weighting, pseudo counts and two-sided representation of amino acid enrichment and depletion. *Nucleic Acids Res.* **40**, W281-7 (2012).